Journal of Hematology & Oncology

RESEARCH

Open Access

Disruption of the sorcin–PAX5 protein–protein interaction induces ferroptosis by promoting the FBXL12-mediated ubiquitination of ALDH1A1 in pancreatic cancer

Yahui Ding[1,2], Yongping Bai[1], Tianyang Chen[1], Sisi Chen[1], Wanjing Feng[1], Shuoqian Ma[2] and Quan Zhang[1,3*]

Abstract

Background Pancreatic cancer is one of the most malignant cancers, and limited therapeutic options are available. The induction of ferroptosis is considered to be a novel, promising strategy that has potential in cancer treatment, and ferroptosis inducers may be new options for eradicating malignant cancers that are resistant to traditional drugs. The exact mechanism underlying the function of sorcin in the initiation and progression of pancreatic cancer remains unclear.

Methods The expression of sorcin in cancer tissues was assessed by analyzing TCGA, GEO and immunohistochemical staining data, and the function of sorcin in the induction of ferroptosis in pancreatic cancer cells was investigated. The mechanism underlying the function of sorcin was revealed through proteomics, co-IP, Ch-IP, and luciferase assays. Natural product screening was subsequently performed to screen for products that interact with sorcin to identify new ferroptosis inducers.

Results We first showed that sorcin expression was positively correlated with the survival and tumor stages of patients with pancreatic cancer, and we revealed that sorcin inhibited ferroptosis through its noncalcium binding function. Furthermore, we discovered that sorcin interacted with PAX5 in the cytoplasm and inhibited PAX5 nuclear translocation, which in turn decreased FBXL12 protein expression and then reduced ALDH1A1 ubiquitination, thus inhibiting ferroptosis. Moreover, an in-house natural product screen revealed that celastrol inhibited the interaction of sorcin and PAX5 by directly binding to the Cys194 residue of the sorcin protein; disruption of the sorcin-PAX5 interaction promoted the nuclear translocation of PAX5, induced the expression of FBXL12, increased the ubiquitylation of ALDH1A1, and eventually induced ferroptosis in pancreatic cancer cells.

Conclusion In this study, we revealed the mechanism of action of sorcin, which is a druggable target for inducing ferroptosis, we identified celastrol as a novel agent that induces ferroptosis, and we showed that disrupting the sorcin-PAX5 interaction is a promising therapeutic strategy for treating pancreatic cancer.

Keywords Sorcin, Ferroptosis, FBXL12, Ubiquitination, PAX5, Celastrol

*Correspondence:
Quan Zhang
zhangquan@nankai.edu.cn

Full list of author information is available at the end of the article

Introduction

Pancreatic cancer is one of the most malignant cancers with the worst prognosis and the highest mortality rate. Although tremendous efforts have been devoted to pancreatic cancer treatment, the mortality rate of pancreatic cancer has shown minimal improvement over the last 40 years. Pancreatic cancer is still a lethal, devastating disease with a five-year survival rate of only 5–8% [1–4]. The main pathological type of pancreatic cancer is pancreatic ductal adenocarcinoma (PDAC), which accounts for 90% of all pancreatic cancer cases [5]. In the United States, PDAC is the fourth leading cause of cancer-related death, and the morbidity and mortality rates associated with PDAC are increasing. It is projected that by 2030, the mortality rate associated with pancreatic cancer will rank second, following only that associated with lung cancer [6]. In China, the mortality rate associated with pancreatic cancer has increased, ranking sixth in 2015. The overall morbidity and mortality rates have also shown increasing trends [7]. The high mortality rate is attributed to the inability to diagnose PDAC in early stages, and this cancer is highly refractory to therapy because of metastasis and recurrence after radiotherapy and chemotherapy [8–10]. Clinical investigations have shown that neither single targeted therapies nor most combination therapies improve the prognosis of pancreatic cancer [11]. As a result, the proposal of novel therapeutic strategies have important implications.

Ferroptosis, which is a term that was coined by Stockwell and colleagues in 2012 [12], is considered an intracellular iron-dependent form of cell death that is different from cellular apoptosis, necrosis, and autophagy [13]. Ferroptosis is characterized by the peroxidation of lipids in cellular membranes, shrunken mitochondria and reduced numbers of mitochondrial cristae [14]. Mechanically, ferroptosis is the antagonistic outcome of cellular metabolism and imbalanced redox homeostasis. The systems that induce ferroptosis include mainly polyunsaturated fatty acid-containing phospholipid (PUFA-PL) synthesis and peroxidation, iron metabolism and mitochondrial metabolism, and these processes eventually induce the accumulation of phospholipid hydroperoxides (PLOOHs) to execute ferroptosis [15]. Moreover, ferroptosis defense systems include mainly the canonical glutathione peroxidase 4 (GPX4)/reduced glutathione (GSH) system and the GPX4-independent system [16]. The canonical GPX4/GSH system consists of a system x_c^- cystine/glutamate antiporter, which transports cystine; thioredoxin reductase 1 (TXNRD1), which meditates GSH biosynthesis; and GPX4, which controls the reduction of PLOOHs to PLOH [15]. The noncanonical GPX4-independent pathway includes the suppressor protein-1/ubiquinol ($FSP1/CoQH_2$) axis [17], the dihydroorotate dehydrogenase/$CoQH_2$ (DHODH//$CoQH_2$) axis [18], and the GTP cyclohydroxylase-1/tetrahydrobiopterin ($GCH1/BH_4$) axis [19].

Increasing evidence suggests that cellular ferroptosis plays significantly important roles in cancer initiation, progression, stemness, metastasis and chemotherapy resistance. The development of resistance to apoptosis-inducing chemotherapy is an important obstacle in cancer therapy [20]. Thus, targeting nonapoptotic mechanisms of cell death could be a novel, promising strategy that has potential in cancer treatment [21]. Early preclinical observations have suggested that some carcinogenic pathways are associated with ferroptosis, making cancer cells highly susceptible to ferroptotic death [22]. It is increasingly recognized that cancer cells that are commonly resistant to conventional therapies or characterized by high metastatic potential might be particularly susceptible to ferroptosis, which provides new opportunities for the treatment of therapy-insensitive tumors [21].

Thus, ferroptosis-based cancer treatment may be a novel option for eradicating malignant cancers that are resistant to traditional drugs. Ferroptosis inducers are expected to overcome the drawbacks of traditional therapeutics [23]. To date, various ferroptosis inducers, including system Xc – inhibitors, GPX4 inhibitors, GSH synthesis inhibitors, FSP1 inhibitors, DHODH inhibitors and GCH1 inhibitors, have been developed and shown to promote ferroptotic cell death [24]. Erastin, sulfasalazine, sorafenib, RSL3, FIN56, withaferin A, ML210 and DPI10 inhibit the canonical GPX4-regulated ferroptosis defense pathway to promote ferroptotic cell death [23, 25]. iFSP1 induces ferroptosis by inhibiting FSP1 enzyme activity and decreasing $CoQH_2$ [26]. icFSP1 regulates ferroptosis by triggering the subcellular relocalization and condensation of FSP1 [27]. FINO2, arteannuin and hemoglobin promote ferroptosis by regulating Fe^{2+} levels and ROS accumulation. However, the in vivo anticancer effects of these ferroptosis inducers need to be further increased. As a result, the development of novel ferroptosis inducers is very important.

ALDH1A1, which is an enzyme that is involved in retinoic acid biosynthesis and redox balance, was identified as a critical biomarker of numerous cancer stem cells and a promising therapeutic target in multiple diseases [28, 29]. In the clinic, high expression of ALDH1A1 is often correlated with poor prognosis [30]. Additionally, ALDH1A1 has important synergistic effects on cancer stemness maintenance, cancer metastasis, cancer angiogenesis, multidrug resistance and antitumor immunity [31, 32]. Furthermore, inhibiting ALDH1A1 can increase the efficacy of KRAS inhibitors by promoting ferroptosis via pH regulation; an ALDH1A1 inhibitor induces the necroptosis of NPC cells; and elevated ALDH1A1 inhibits the necroptosis of tumor cells [33, 34]. These findings

suggest that ALDH1A1 is a promising target for cancer therapy.

Soluble resistance-related calcium binding protein (Sorcin), which is a soluble penta EF-hand calcium-binding protein (22 kDa), plays important roles in the regulation of calcium homeostasis, cancer development, and multidrug resistance (MDR) [35–38]. In addition, sorcin was shown to regulate the tumorigenesis, invasion, and migration of different tumor cells by regulating various key molecules that are involved in these processes, such as NF-κB, CTSZ, STAT3, Akt, ERK1/2, VEGF, MMPs, and caspases, as well as signaling pathways, including the ERK, MAPK/ERK, and PI3K/Akt pathways [39–41]. In addition, sorcin mediates pyroptosis in hepatocellular carcinoma and interacts with the NLRP3 inflammasome [42]. However, the exact mechanism of action of sorcin in the initiation, progression and multidrug resistance of many cancers remains unclear. Here, we first showed that sorcin expression was positively correlated with the survival and tumor stages of patients with pancreatic cancer, and we revealed that sorcin inhibited ferroptosis in a Ca^{2+}-independent manner. Furthermore, we discovered that sorcin interacted with PAX5 in the cytoplasm and inhibited PAX5 nuclear translocation, which in turn decreased the protein expression of FBXL12 and then reduced the ubiquitination of ALDH1A1, thus inhibiting ferroptosis. Moreover, an in-house natural product screen identified celastrol as an inhibitor of the protein–protein interaction between sorcin and PAX5 that induced ferroptosis in pancreatic cancer cells. Our data revealed a mechanism underlying the tumorigenic effects of sorcin, which functions as a ferroptosis suppressor, and suggest that the sorcin-PAX5 interaction is a promising therapeutic target for the treatment of pancreatic cancer.

Results

Sorcin was overexpressed in cancer tissues and its overexpression was correlated with patient survival

To evaluate the potential relationship between sorcin function and cancer progression, we analyzed sorcin expression in the TCGA database. The results revealed that patients in the high sorcin expression group exhibited significantly shorter overall survival (OS), disease-specific survival (DSS), progression-free survival (PFS) and recurrence-free interval (RFI) than those in the low sorcin expression group (Fig. 1A). Moreover, sorcin gene expression was greatly increased in tumor tissues compared with normal tissues, as shown in the GSE15471, GSE62165, GSE62452 and GSE28735 datasets (Fig. 1B). Moreover, a stage-specific analysis was performed to determine the correlation between sorcin protein levels and the clinical stage of pancreatic cancer. The immunohistochemical staining results revealed that the sorcin protein was overexpressed in pancreatic cancer tissues compared with normal pancreatic tissues, and higher sorcin protein levels were significantly associated with higher histological grades (Fig. 1C and D). In addition, an immunohistochemical assay on a tissue microarray that included samples from 98 primary pancreatic cancer patients revealed that high sorcin protein levels were significantly associated with poor overall survival ($P < 0.05$) (Fig. 1E). These results revealed that sorcin might participate in pancreatic cancer progression and may represent a novel prognostic index for predicting the progression of pancreatic cancer or the overall survival of patients with pancreatic cancer.

Sorcin promoted pancreatic cancer progression

The function of sorcin in pancreatic cancer is still unclear. To analyze the effect of sorcin on cancer progression, the expression levels of the endogenous sorcin gene in pancreatic cancer cell lines were measured. The results indicated that sorcin was highly expressed in PANC-1, Capan-2 and AsPC-1 cells (Fig. 2A). ALDH1A1, which promotes the self-renewal of cancer stem cells (CSCs) and contributes to cancer progression, is considered the most important biomarker of CSCs. Our results indicated that ALDH1A1 expression was significantly reduced after sorcin knockdown but obviously increased after sorcin overexpression in PANC-1, AsPC-1, Capan-2, PaTu8988T and MIA Paca-2 cells (Fig. 2B). Next, we examined the effects of silencing sorcin on the migration and invasion of pancreatic cancer cells. The results demonstrated that the migration and invasion rates were obviously inhibited after sorcin knockdown but increased after sorcin overexpression (Fig. 2C and E, Figure S1). Tumorsphere formation analysis indicated that sorcin knockdown significantly reduced tumorsphere numbers, whereas sorcin overexpression markedly increased tumorsphere numbers (Fig. 2F). Additionally, the percentage of $ALDH^+$ PANC-1 and Capan-2 cells clearly decreased after sorcin knockdown (Fig. 2G and J). Moreover, an animal assay revealed that knockdown of sorcin significantly inhibited pancreatic tumor growth (Fig. 2K and L), and an IHC assay demonstrated that ALDH1A1 expression was clearly reduced in the sorcin-knockdown group (Fig. 2M). These findings suggested that sorcin promoted cancer progression and increased ALDH1A1 abundance.

Sorcin was identified as a suppressor of ferroptosis

The ALDH1 family plays important roles in the detoxification of aldehydes produced from lipid peroxidation, which accumulate to execute ferroptosis; this suggested that sorcin could mediate ferroptosis by regulating ALDH1A1 levels. We first examined the effects of silencing sorcin on the level of lipid peroxidation, which is

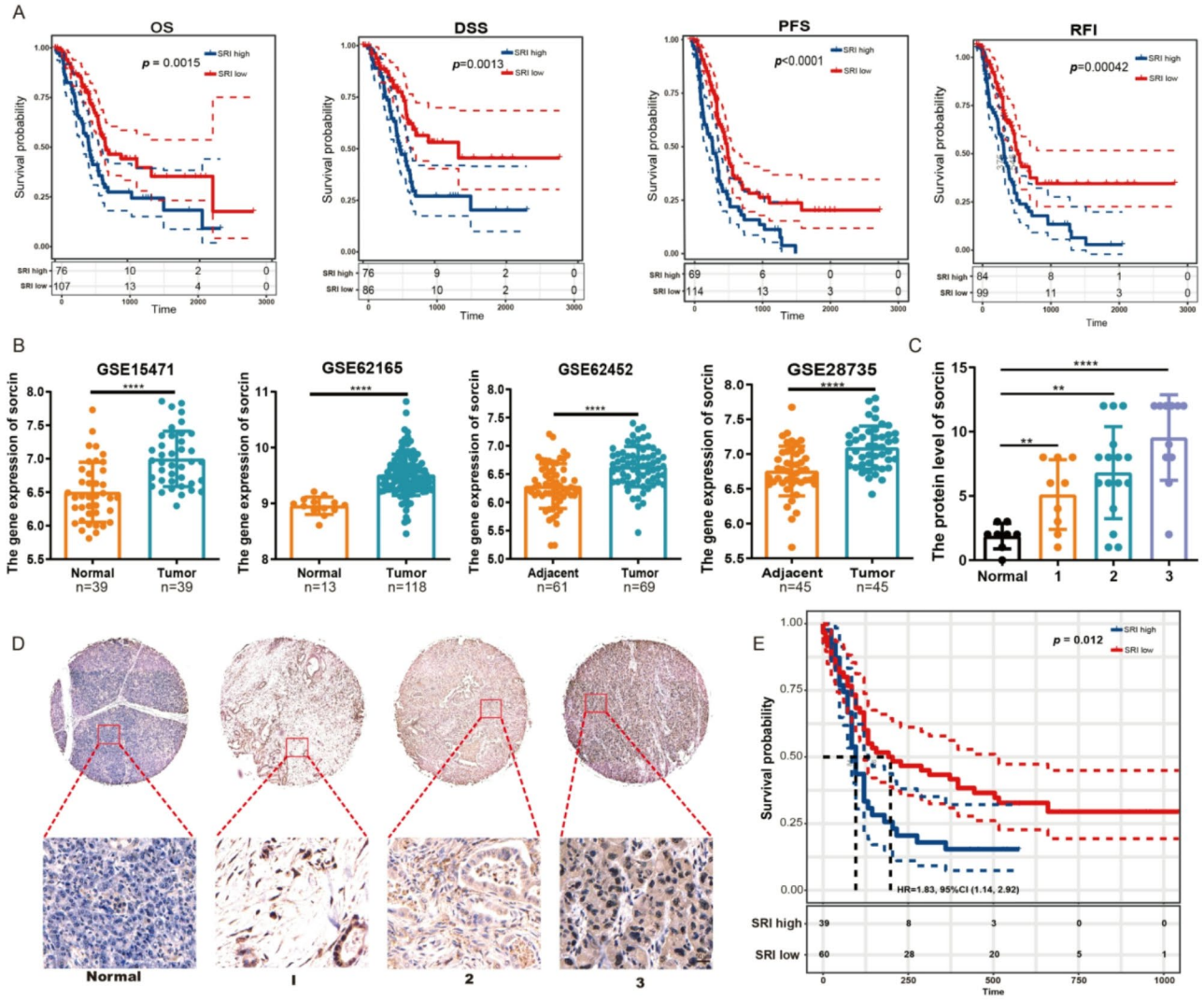

Fig. 1 Sorcin was overexpressed in cancer tissues and its overexpression was correlated with survival. (**A**) Survival analysis, including analysis of overall survival (OS), disease-specific survival (DSS), progression-free survival (PFS) and the recurrence-free interval (RFI), of patients with pancreatic cancer with different sorcin expression levels in the TCGA database. (**B**) Sorcin gene expression levels in normal and tumor tissues in GEO datasets, including the GSE15471, GSE62165, GSE62452 and GSE28735 datasets. (**C**) IHC analysis of sorcin protein levels in pancreatic cancer tissues of different clinical stages. (**D**) Representative images of immunohistochemical staining for sorcin protein expression in normal pancreatic tissues and pancreatic cancer tissues of different stages. (**E**) Overall survival analysis of 98 patients with pancreatic cancer stratified according to sorcin expression

a cardinal feature of ferroptosis. The results indicated that lipid ROS levels were clearly increased after sorcin knockdown but decreased after sorcin overexpression in PANC-1 and Capan-2 cells (Fig. 3A and H). These results suggested that sorcin knockdown promoted ferroptosis and that sorcin overexpression inhibited ferroptosis. Malondialdehyde (MDA), which is a product of membrane lipid peroxidation that is positively associated with ferroptosis, was strongly increased after sorcin knockdown but obviously reduced after sorcin overexpression (Fig. 3I and J). Furthermore, the observation of mitochondrial morphology by electron microscopy suggested that after sorcin knockdown, the number of mitochondrial cristae was reduced, the mitochondria were darkly stained, and the mitochondria were wrinkled; these phenomena are hallmark morphological features of ferroptosis (Fig. 3K).

To investigate the multiple forms of cell death that are induced by sorcin, we assessed the apoptosis of sorcin-knockdown and sorcin-overexpressing cells by flow cytometry. The results revealed no significant change in the rate of apoptosis, which suggested that the primary function of sorcin was not to induce apoptosis (Fig. 3L). The pyroptosis-related protein GSDMD-N-terminal domain (GSDMD-N) is the ultimate executor of pyroptosis. We then analyzed the GSDMD-N levels in sorcin-knockdown cells by Western blotting, and the results revealed that the GSDMD-N levels were strongly

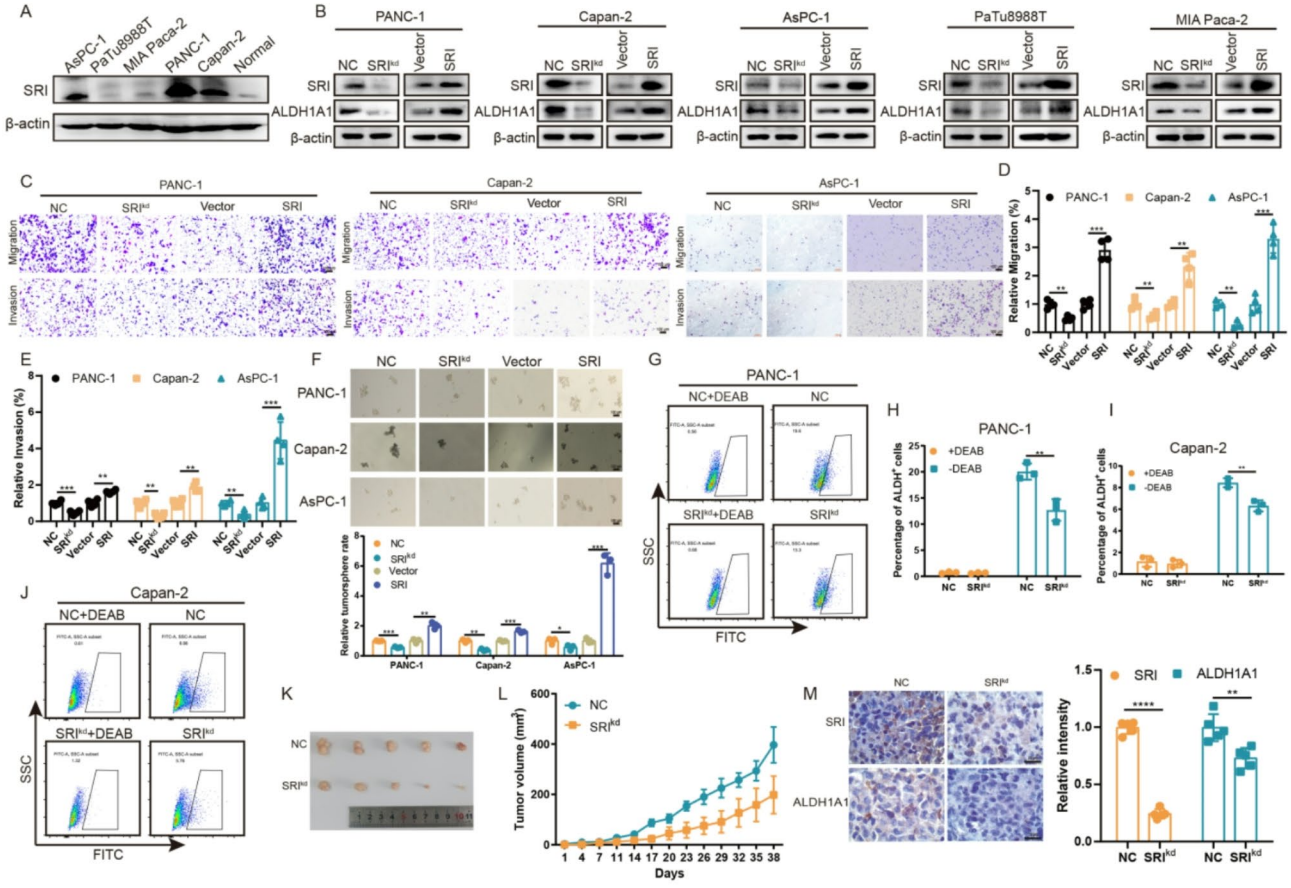

Fig. 2 Sorcin promoted pancreatic cancer progression. **(A)** The expression level of sorcin in pancreatic cancer cells. (**B**) Western blotting analysis of sorcin and ALDH1A1 expression in PANC-1, AsPC-1, Capan-2, PaTu8988T and MIA Paca-2 pancreatic cancer cells after sorcin was knocked down by shRNA or overexpressed. (**C**) Representative images of the migration and invasion of PANC-1, Capan-2 and AsPC-1 cells after sorcin was knocked down by shRNA or overexpressed. (**D-E**) Statistical analysis of the migration and invasion of PANC-1, Capan-2 and AsPC-1 cells after sorcin was knocked down by shRNA or overexpressed. (**F**) Representative images and statistical analysis of the tumorsphere formation rate after sorcin knockdown or overexpression. (**G**-**H**) Representative images and statistical analysis of ALDH$^+$ PANC-1 cells after sorcin knockdown. (**I**-**J**) Representative images and statistical analysis of ALDH$^+$ Capan-2 cells after sorcin knockdown. (**K**-**L**) Images and growth rates of tumors from mice engrafted with sorcin-knockdown PANC-1 cells, $n=5$. (**M**) Representative images of immunohistochemical staining and statistical analysis of sorcin and ALDH1A1 expression levels in xenograft tumor tissues

increased after sorcin knockdown; these results indicated that sorcin knockdown induced pyroptosis (Fig. 3M). Recent studies have revealed that crosstalk occurs between different forms of programmed cell death. Next, we analyzed whether the promotion of GSDMD-N cleavage was induced by ferroptosis. The results suggested that the ferroptosis inhibitor liproxstatin-1 clearly inhibited the sorcin knockdown-induced cleavage of GSDMD-N, which suggested that sorcin knockdown induced pyroptosis through ferroptosis (Fig. 3N).

Sorcin decreased susceptibility to ferroptosis

To further confirm that sorcin knockdown promoted ferroptosis, we determined whether the genetic suppression of sorcin expression enhanced susceptibility to ferroptosis. In this process, we used RSL3 and erastin, which are two specific inducers of ferroptosis. The results showed that sorcin knockdown markedly amplified the RSL3- or erastin-induced accumulation of lipid ROS (Fig. 4A and D). Additionally, sorcin overexpression obviously suppressed the RSL3- or erastin-induced accumulation of lipid ROS (Fig. 4E and H). Furthermore, sorcin knockdown clearly increased cell death after treatment with ferroptosis inducers (Fig. 4I), whereas sorcin overexpression reduced death (Fig. 4J). To investigate whether the ability of sorcin to suppress ferroptosis resulted in the metastasis of pancreatic cancer, a transwell assay was performed with the combination of sorcin knockdown with ferroptosis inducers or ferroptosis inhibitors. The combination of sorcin knockdown with ferroptosis inducers had synergistic effects on migration and invasion, whereas the combination of sorcin knockdown with ferroptosis inhibitors had antagonistic effects on migration and invasion (Fig. 4K and N). These results suggested that sorcin knockdown increased the susceptibility to ferroptosis induced by ferroptosis inducers.

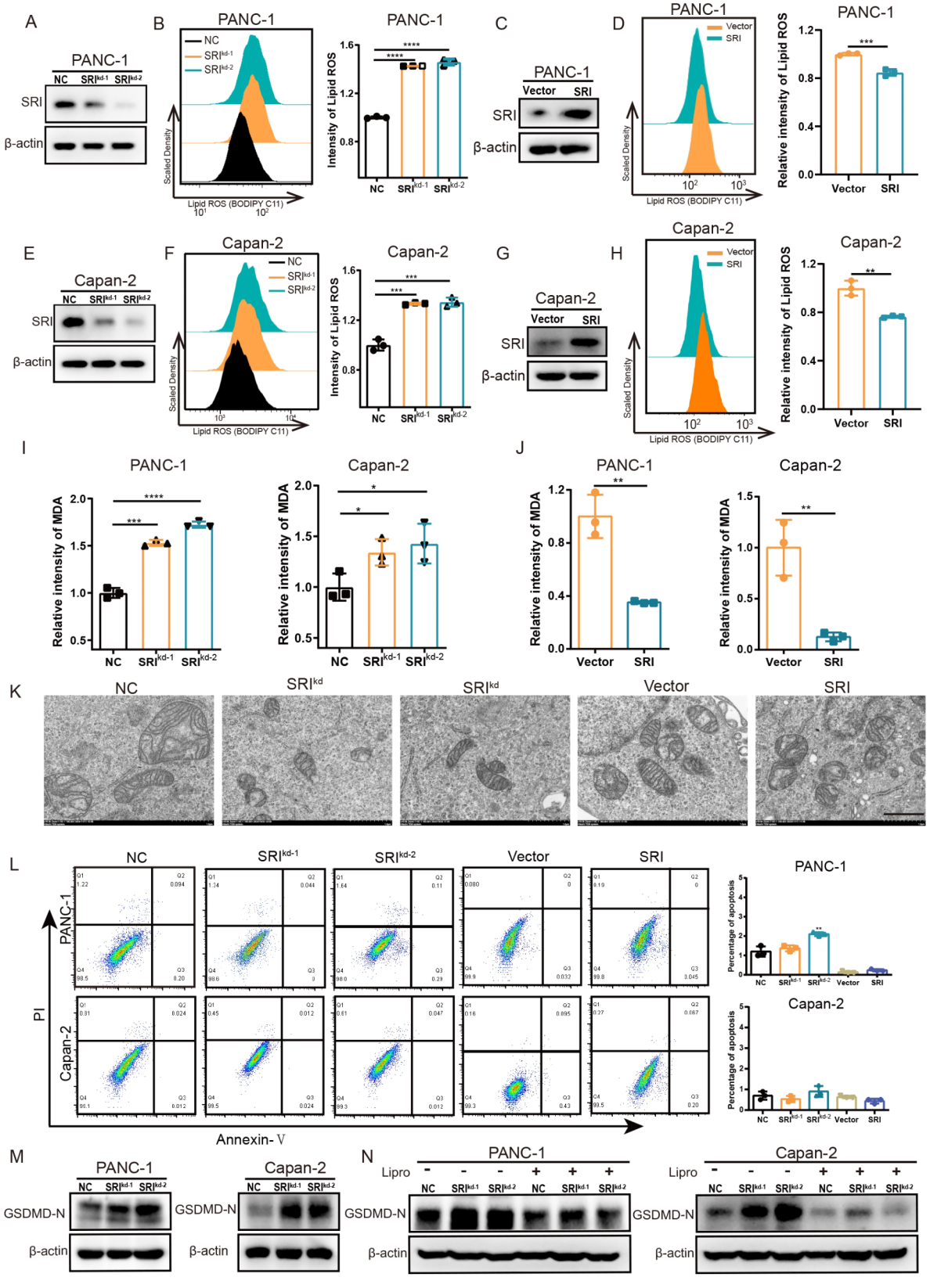

Fig. 3 (See legend on next page.)

(See figure on previous page.)

Fig. 3 Sorcin was identified as a suppressor of ferroptosis. (**A**-**B**) Lipid ROS levels in PANC-1 cells after sorcin was knocked down by shRNA. (**C**-**D**) Lipid ROS levels in PANC-1 cells after sorcin was overexpressed. (**E**-**F**) Lipid ROS levels in Capan-2 cells after sorcin was knocked down by shRNA. (**G**-**H**) Lipid ROS levels in Capan-2 cells after sorcin was overexpressed. (**I**) The intensity of malondialdehyde in PANC-1 and Capan-2 cells after sorcin was knocked down by shRNA. (**J**) The intensity of malondialdehyde in PANC-1 and Capan-2 cells after sorcin overexpression. (**K**) Changes in mitochondrial morphology observed by transmission electron microscopy after sorcin was knocked down by shRNA or overexpressed. (**L**) Representative images and statistical analysis of the apoptosis of PANC-1 and Capan-2 cells after sorcin was knocked down by shRNA or overexpressed. (**M**) GSDMD-N protein levels in PANC-1 and Capan-2 cells after sorcin was knocked down by shRNA. (**N**) GSDMD-N protein levels in sorcin-knockdown cells after incubation with liproxstatin-1

Sorcin suppressed ferroptosis by regulating ALDH1A1 abundance

To further determine whether sorcin regulates ferroptosis by regulating ALDH1A1 expression, we first investigated the effect of ALDH1A1 on ferroptosis. We then constructed stable ALDH1A1-knockdown cell lines and detected lipid ROS with a fluorescent probe and flow cytometry. The results suggested that lipid ROS levels were strongly increased after ALDH1A1 knockdown in PANC-1 and Capan-2 cells (Fig. 5A and D). The malondialdehyde levels were also significantly increased after ALDH1A1 expression was suppressed (Fig. 5E). The Transwell results indicated that the migration and invasion of pancreatic cancer cells were obviously decreased after ALDH1A1 knockdown (Fig. 5F and G). Furthermore, suppression of ALDH1A1 expression clearly amplified the cell death that was induced by ferroptosis inducers (Fig. 5H). Additionally, lipid ROS intensity assays suggested that ALDH1A1 knockdown further increased erastin-induced and RSL3-induced increases in lipid ROS levels (Fig. 5I and J), and this effect was negatively correlated with ferroptosis inducer-mediated cell viability (Fig. 5K). These results indicate that ALDH1A1 was involved in ferroptosis and that the knockdown of ALDH1A1 induced ferroptosis.

On the basis of the results described above, we hypothesized that ALDH1A1 enzyme inhibitors may also induce ferroptosis in pancreatic cancer cells. As a result, ALDH1A1 enzyme inhibitors, including disulfiram (DSF) and 4-diethylaminobenzaldehyde (DEAB), were selected. The results suggested that DSF and DEAB both increased the lipid ROS intensity in a dose-dependent manner, which further demonstrated the effect of ALDH1A1 on ferroptosis (Fig. 5L and M). Moreover, the results of the cell viability assays suggested that DSF and DEAB promoted erastin-induced and RSL3-induced cell death (Fig. 5N and P).

To further confirm the regulatory relationship between sorcin and ALDH1A1 in the induction of ferroptosis, we transfected an ALDH1A1-overexpressing plasmid into sorcin-knockdown cells and measured lipid ROS levels by flow cytometry. These results suggested that ALDH1A1 expression can rescue sorcin knockdown-induced ferroptosis, which suggested that sorcin knockdown induced ferroptosis by inhibiting ALDH1A1 abundance (Fig. 5Q and R).

These data demonstrated that ALDH1A1 was involved in ferroptosis and that sorcin mediated ferroptosis by regulating ALDH1A1 abundance.

Sorcin regulated ALDH1A1 levels through its noncalcium binding function

Sorcin participates in the regulation of calcium homeostasis by binding to calcium. Therefore, silencing sorcin would be expected to increase the level of intracellular Ca^{2+}. We compared endogenous calcium levels after sorcin knockdown, and the results showed that the knockdown of sorcin could increase the calcium levels (Fig. 6A and B). The addition of the calcium chelating agent BAPTA-AM reduced ALDH1A1 expression. Moreover, the addition of BAPTA-AM increased the sorcin knockdown-mediated inhibition of ALDH1A1 expression (Fig. 6C). These results suggested that Ca^{2+} might promote ALDH1A1 expression. Since the knockdown of sorcin significantly reduced the expression of ALDH1A1, sorcin performed a noncalcium binding function in regulating the ALDH1A1 level. However, the detailed mechanism is still not clear.

To further elucidate the mechanism by which sorcin regulates ALDH1A1 abundance, a proteomics assay was performed, and the proteins whose expression changed the most were analyzed. The results suggested that FBXL12 expression was most significantly changed after sorcin knockdown compared with negative control, and this result indicated that sorcin may regulate FBXL12 expression (Fig. 6D). The gene expression assay revealed that FBXL12 gene expression was significantly increased after sorcin knockdown but decreased after sorcin overexpression (Fig. 6E). Western blotting analysis demonstrated that sorcin knockdown increased FBXL12 protein expression and that sorcin overexpression decreased FBXL12 protein expression in PANC-1, Capan-2 and AsPC-1 cells (Fig. 6F and I). We then explored FBXL12 expression in primary pancreatic cancer tissues and adjacent tissues via an IHC assay, and the results suggested that FBXL12 was expressed at lower levels in cancer tissues than in adjacent normal tissues (Fig. 6J and K). Furthermore, the clinical correlation between FBXL12 gene expression and survival time in the TCGA database was analyzed. The results revealed that low FBXL12 gene expression was significantly associated with poor disease-specific survival (DSS), overall survival (OS), progression-free interval (PFI), progression-free survival (PFS)

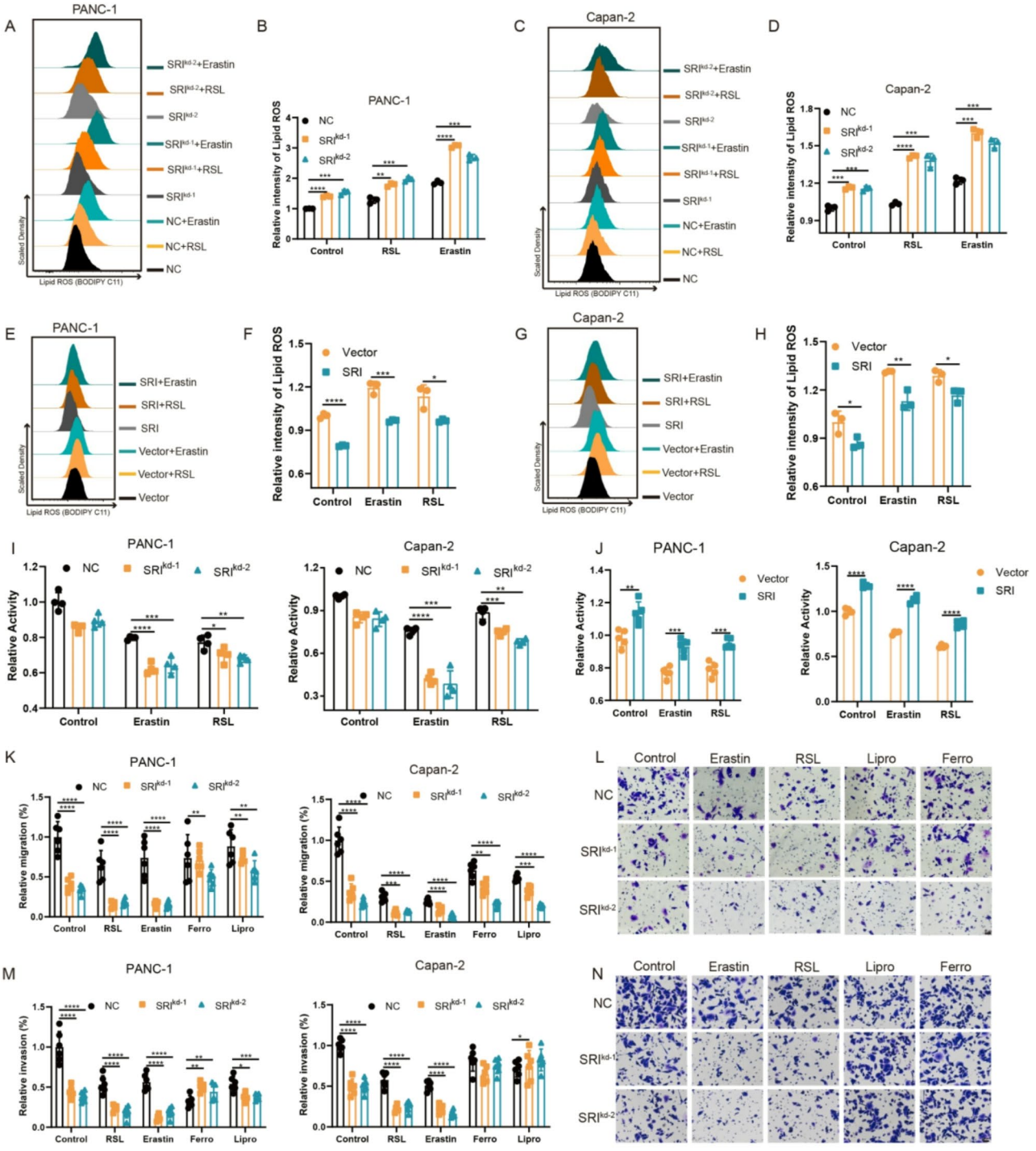

Fig. 4 Sorcin decreased susceptibility to ferroptosis. (**A**-**D**) Representative images and statistical analysis of lipid ROS levels in shRNA-induced sorcin-knockdown cells after treatment with RSL3 or erastin for 48 h. (**E**-**H**) Representative images and statistical analysis of lipid ROS levels in sorcin-overexpressing cells after treatment with RSL3 or erastin for 48 h. (**I**) Analysis of the viability of shRNA-induced sorcin-knockdown cells after treatment with RSL3 or erastin for 36 h. (**J**) Analysis of the viability of sorcin-overexpressing cells after treatment with RSL3 or erastin for 48 h. (K) Statistical analysis of the migration of the indicated PANC-1 and Capan-2 cells after treatment with RSL3 (0.5 μM), erastin (1 μM), Ferro (5 μM), or Lipro (2 μM) for 48 h. (L) Representative images of the migration of the indicated Capan-2 cells. (**M**) Statistical analysis of the invasion of the indicated PANC-1 and Capan-2 cells after treatment with RSL3 (0.5 μM), erastin (1 μM), Ferro (5 μM), or Lipro (2 μM) for 48 h. (**N**) Representative images of cell invasion of the indicated Capan-2 cells

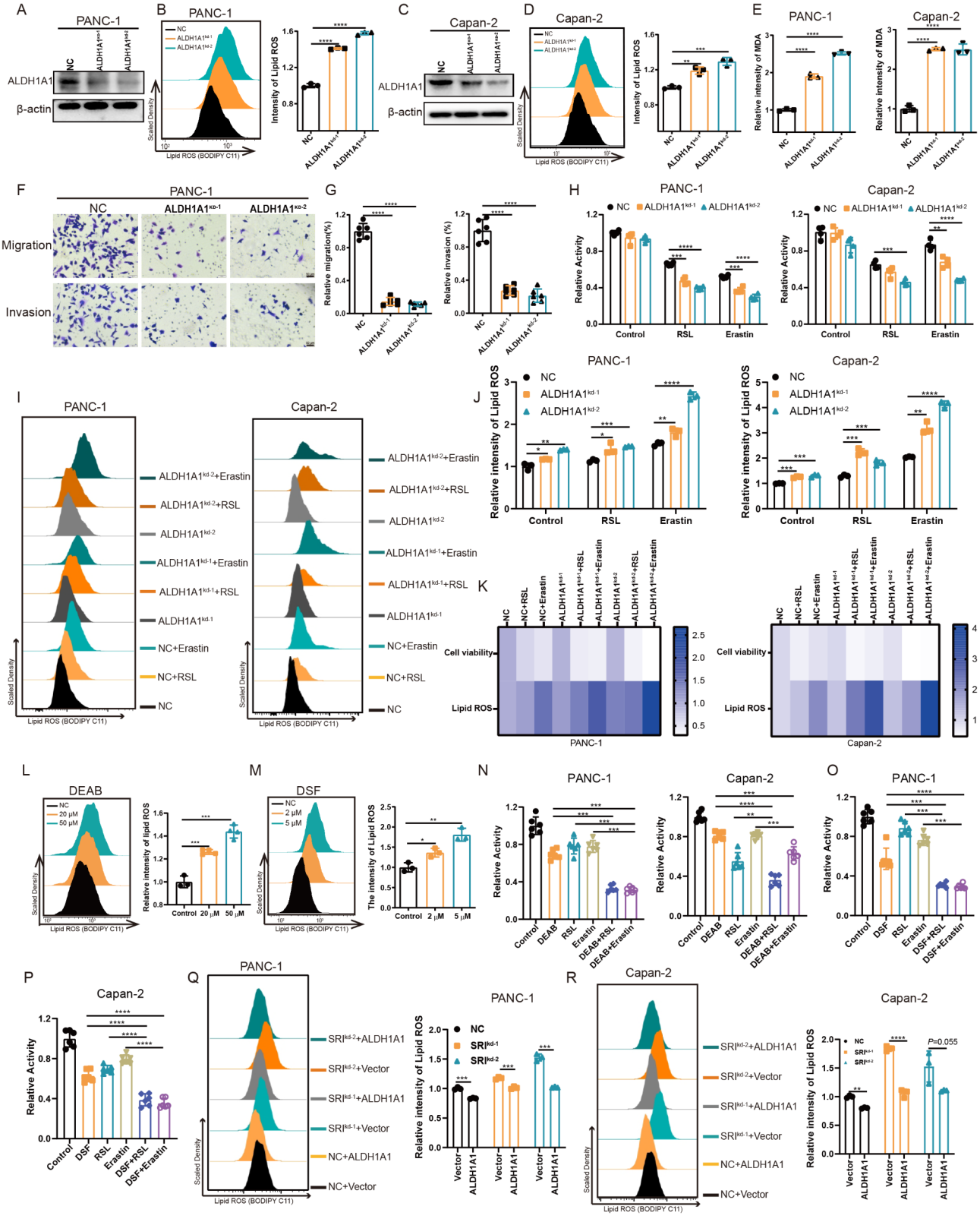

Fig. 5 (See legend on next page.)

(See figure on previous page.)

Fig. 5 Sorcin suppressed ferroptosis by regulating ALDH1A1 abundance. (**A**) Western blotting analysis of ALDH1A1 protein levels in negative control and shRNA-induced ALDH1A1-knockdown PANC-1 cells. (**B**) Representative images and statistical analysis of lipid ROS intensity in PANC-1 cells after ALDH1A1 was knocked down by shRNA. (**C**) Western blotting analysis of ALDH1A1 protein levels in negative control and ALDH1A1-knockdown Capan-2 cells. (**D**) Representative images and statistical analysis of lipid ROS intensity in Capan-2 cells after ALDH1A1 was knocked down by shRNA. (**E**) Analysis of malondialdehyde intensity in PANC-1 and Capan-2 cells after ALDH1A1 was knocked down by shRNA. (**F**) Representative images of PANC-1 cell migration and invasion after ALDH1A1 was knocked down by shRNA. (**G**) Statistical analysis of PANC-1 cell migration and invasion after ALDH1A1 was knocked down by shRNA. (**H**) Analysis of the viability of the indicated PANC-1 and Capan-2 cells after treatment with RSL3 or erastin for 36 h. (**I**-**J**) Representative images and statistical analysis of lipid ROS levels in the indicated PANC-1 and Capan-2 cells after treatment with RSL3 (0.5 μM) or erastin (1 μM) for 48 h. (**K**) Comparison of the viability and lipid ROS levels of the indicated cells after treatment with RSL3 or erastin. (**L**) Representative images and statistical analysis of lipid ROS levels after treatment with DEAB for 48 h. (**M**) Representative images and statistical analysis of lipid ROS levels after treatment with disulfiram (DSF) for 48 h. (**N**) Viability of the indicated PANC-1 and Capan-2 cells treated with DEAB combined with RSL3 or erastin for 72 h. (**O**-**P**) Viability of the indicated PANC-1 and Capan-2 cells treated with DSF combined with RSL3 or erastin for 72 h. (**Q**) Representative images and statistical analysis of lipid ROS levels in sorcin-knockdown PANC-1 cells after transfection with the ALDH1A1 plasmid. (**R**) Representative images and statistical analysis of lipid ROS levels in sorcin-knockdown Capan-2 cells after transfection with the ALDH1A1 plasmid

and the recurrence-free interval (RFI) (Fig. 6L). These results indicated that sorcin regulated ALDH1A1 protein levels by altering FBXL12 gene expression and that FBXL12 was negatively correlated with tumorigenesis.

FBXL12 inhibited pancreatic cancer progression by inhibiting ALDH1A1 levels

To further elucidate the function of FBXL12 in pancreatic cancer progression, Transwell, tumorsphere and Western blotting assays were performed. The Transwell assay results revealed that the migration of pancreatic cancer cells was strongly increased after FBXL12 knockdown but reduced after FBXL12 overexpression (Fig. 7A and B). The tumorsphere formation rate was significantly increased after FBXL12 knockdown but decreased after FBXL12 overexpression (Fig. 7C and D). Western blotting analysis revealed that the ALDH1A1 levels were increased after FBXL12 knockdown but reduced after FBXL12 overexpression (Fig. 7E and F).

To determine whether sorcin regulated ALDH1A1 levels to induce ferroptosis via FBXL12, a rescue experiment was performed. FBXL12 siRNA was transfected into sorcin-knockdown cells, after which the ALDH1A1 levels and lipid ROS levels were analyzed. The flow cytometry results suggested that FBXL12 knockdown suppressed sorcin knockdown-induced increase in lipid ROS levels, which suggested that FBXL12 knockdown suppressed sorcin knockdown-induced ferroptosis (Fig. 7G and H). Furthermore, the Western blotting results indicated that FBXL12 knockdown reversed the sorcin knockdown-induced reducing in ALDH1A1 levels (Fig. 7I). These results indicated that sorcin regulated ALDH1A1 abundance through FBXL12.

FBXL12 mediated ALDH1A1 ubiquitination

FBXL12 plays important roles in a wide variety of cellular functions by mediating ubiquitination. To determine whether FBXL12 mediated ALDH1A1 ubiquitylation in pancreatic cancer cells, we treated pancreatic cancer cells with the proteasome inhibitor MG132 and the protein synthesis inhibitor cycloheximide (CHX). The results showed that ALDH1A1 protein levels increased after treatment with MG132 in a time-dependent and dose-dependent manner (Fig. 8A and C, S2A), whereas ALDH1A1 protein levels decreased after treatment with cycloheximide in a time-dependent and dose-dependent manner (Fig. 8B and D, S2B); these results suggested that ALDH1A1 was modified by ubiquitination. Moreover, FBXL12 knockdown inhibited the effect of cycloheximide on ALDH1A1 degradation, indicating that FBXL12 is involved in the ubiquitination and degradation of ALDH1A1 (Fig. 8E and F). To further analyze whether ALDH1A1 ubiquitylation was mediated by FBXL12, an immunofluorescence assay and a coimmunoprecipitation assay were performed. Immunofluorescence analysis revealed that ALDH1A1 colocalized with FBXL12 in PANC-1 and Capan-2 cells (Fig. 8G). Additionally, the interaction between FBXL12 and ALDH1A1 after overexpression of a Flag-tagged FBXL12 protein was analyzed by coimmunoprecipitation with an anti-Flag antibody; the results suggested that FBXL12 directly interacted with ALDH1A1 (Fig. 8H). The interaction between FBXL12 and ALDH1A1 was further confirmed by overexpressing an HA-tagged ALDH1A1 protein and performing coimmunoprecipitation with an anti-HA antibody (Fig. 8I). Moreover, we verified that the level of ubiquitinated ALDH1A1 was obviously decreased after FBXL12 knockdown but increased after FBXL12 overexpression (Fig. 8J). Finally, coimmunoprecipitation analysis with an anti-ubiquitin antibody revealed that ALDH1A1 was ubiquitinated (Fig. 8K). Taken together, these results suggested that sorcin regulated the gene expression of FBXL12 and that FBXL12 is an authentic E3 ligase that regulated the ubiquitination and degradation of ALDH1A1.

Sorcin mediated the nuclear translocation of PAX5 to regulate FBXL12 transcription

To identify the specific mechanism by which sorcin regulated FBXL12 to affect ALDH1A1 levels, proteomics results were analyzed. The GO analysis results indicated that the primary functions of the sorcin protein might

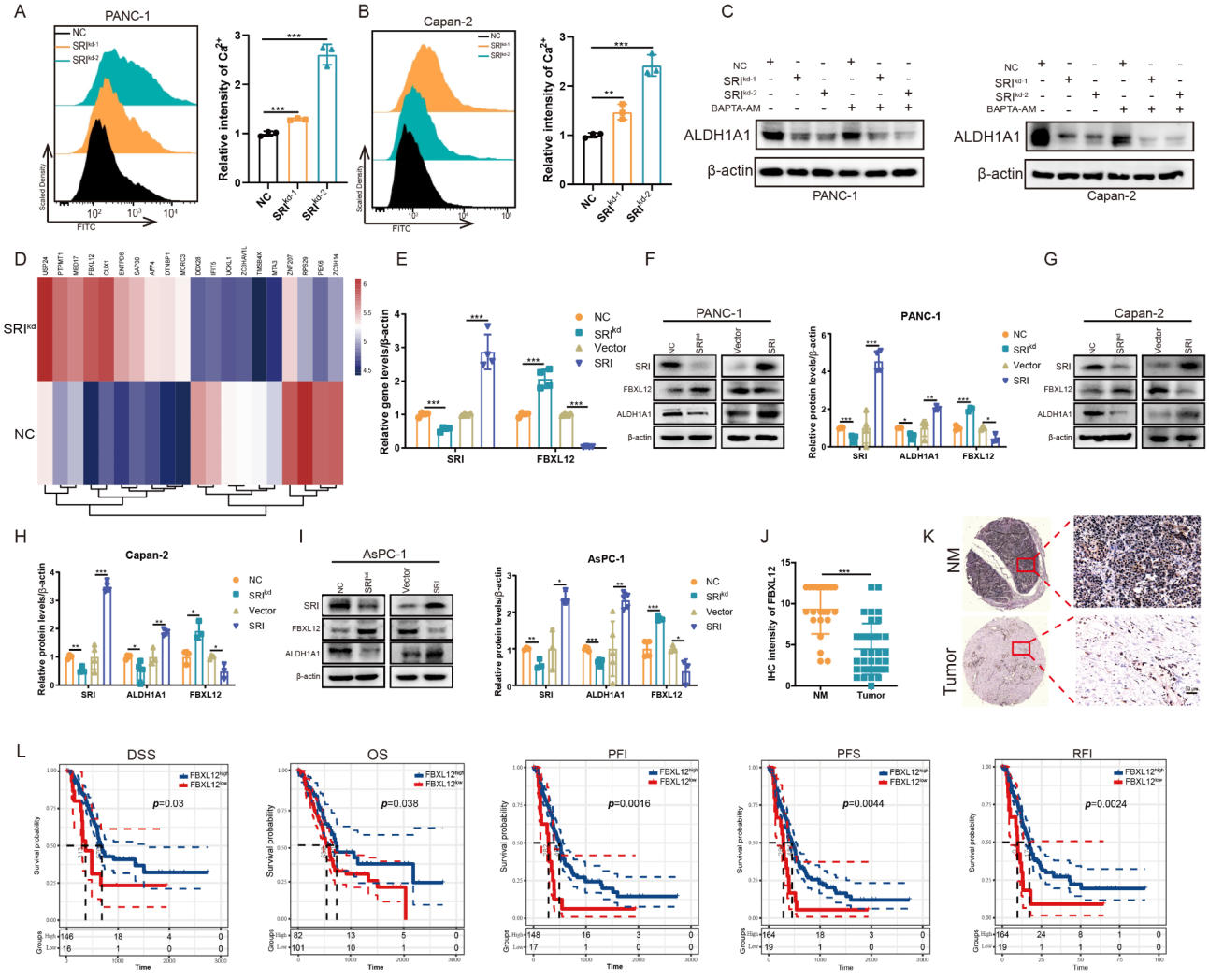

Fig. 6 Sorcin regulated ALDH1A1 levels through its noncalcium binding function

be interacting with proteins and transcription factors (Fig. 9A and B). As a result, we hypothesized that sorcin would bind to some transcription factors that regulate FBXL12 transcription. However, the transcription factor that regulates FBXL12 has rarely been studied. To explore the transcription factors that regulate the gene expression of FBXL12, fragments of the FBXL12 promoter sequence named P1 (nucleotides −1750 - +251), P2 (nucleotides −1750 - -1250), P3 (nucleotides −1250 - -750), P4 (nucleotides −1750 - -750), P5 (nucleotides −1750 - -492), and P6 (nucleotides −492 - +251) were inserted into the pGL3-basic vector (Fig. 9C). The luciferase signals of P6 were significantly greater than the luciferase signals of P1, P2, P3, P4 and P5 in PANC-1 and Capan-2 cells (Fig. 9D). These results indicated that P6 was the core promoter region. We predicted the transcription factor that regulates FBXL12 expression by analyzing the core promoter region with http://alggen.lsi.upc.es/ (Fig. 9E). The transcription factor PAX5 exhibited the highest frequency of occurrence, and PAX5 was hypothesized to be the main transcription factor that regulates FBXL12 expression. Furthermore, the binding site of PAX5 in the promoter was determined by a Ch-IP assay. The results suggested that site 2 and site 4 were the main binding sites of PAX5 (Fig. 9F). Moreover, luciferase activity was greatly reduced after the PAX5 binding site 2 and site 4 were mutated, and site 2 played a more important role than site 4 (Fig. 9G). Therefore, PAX5 mainly bound to site 2 in the promoter of FBXL12. Western blotting analysis also revealed that PAX5 knockdown clearly decreased FBXL12 protein expression, whereas PAX5 overexpression increased FBXL12 protein expression in PANC-1, AsPC-1 and Capan-2 cells (Fig. 9H).

However, how sorcin regulates the expression of FBXL12 via PAX5 still needs to be explored. The above results prompted us to hypothesize that sorcin might interact with PAX5 and affect its nuclear translocation. First, we detected the interaction between PAX5 and

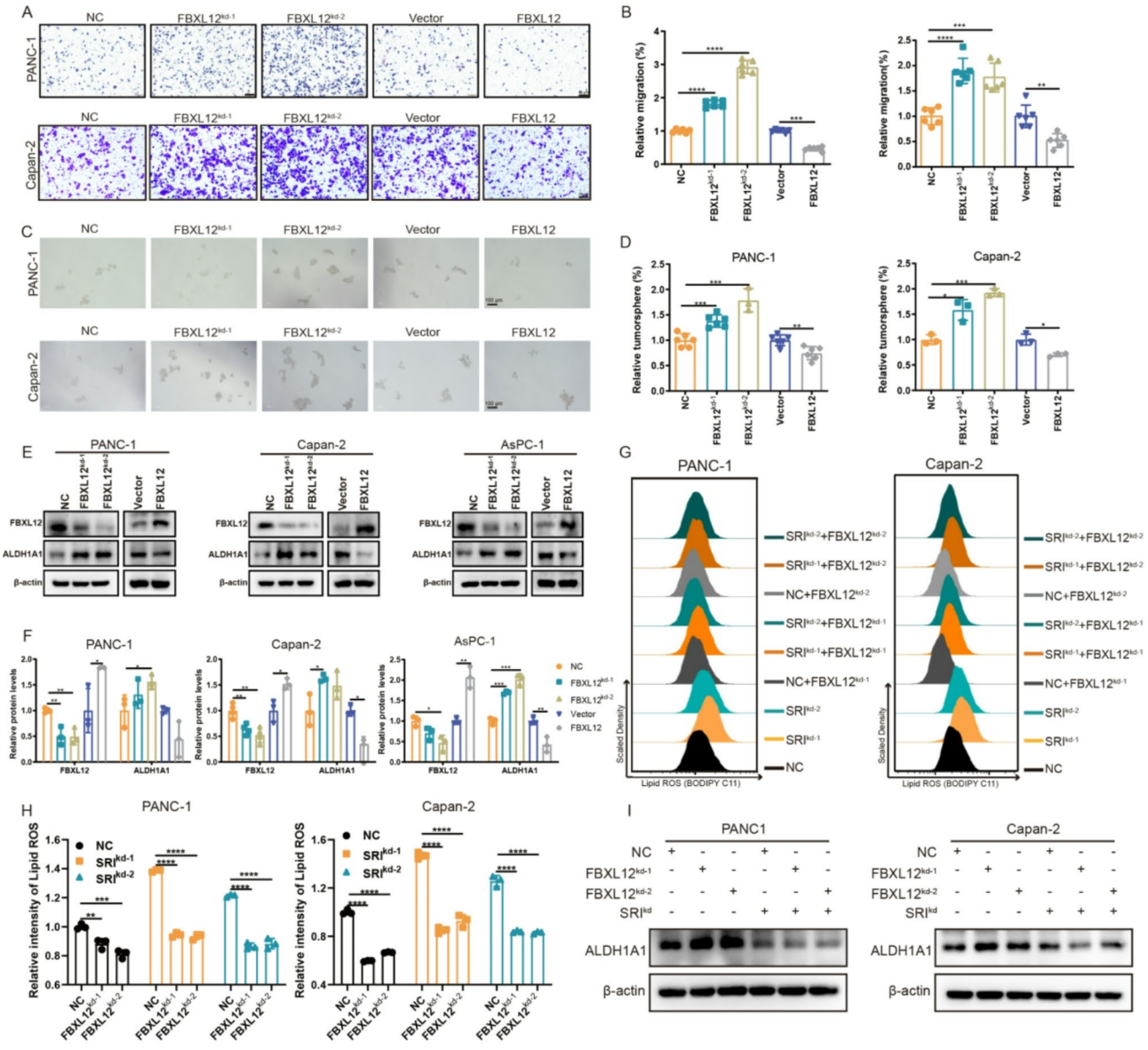

Fig. 7 FBXL12 inhibited pancreatic cancer progression by inhibiting ALDH1A1 levels. (**A**) Representative images of PANC-1 and Capan-2 cell migration after FBXL12 was knocked down by siRNA or overexpressed. (**B**) Statistical analysis of cell migration after FBXL12 was knocked down by siRNA or overexpressed. (**C**) Representative images of tumorsphere formation by PANC-1 and Capan-2 cells after FBXL12 was knocked down by siRNA or overexpressed. (**D**) Statistical analysis of tumorsphere formation after FBXL12 was knocked down by siRNA or overexpressed. (**E**-**F**) Western blotting analysis and statistical analysis of FBXL12 and ALDH1A1 expression in PANC-1, Capan-2 and AsPC-1 cells after FBXL12 was knocked down by siRNA or overexpressed. (**G**) Representative images of lipid ROS levels in sorcin-knockdown cells after transfection with FBXL12 siRNAs. (**H**) Statistical analysis of lipid ROS levels in sorcin-knockdown cells after transfection with FBXL12 siRNAs. (**I**) Western blotting analysis of ALDH1A1 expression in sorcin-knockdown cells after transfection with FBXL12 siRNAs

sorcin after the overexpression of a Flag-tagged sorcin protein by performing a coimmunoprecipitation assay with an anti-Flag antibody, and the results suggested that PAX5 directly interacted with sorcin (Fig. 9I). Furthermore, the interaction between PAX5 and sorcin after Flag-tagged PAX5 protein overexpression was confirmed by performing a coimmunoprecipitation assay with an anti-Flag antibody (Fig. 9J). We then assessed the nuclear translocation of PAX5 by immunofluorescence, and the results revealed that the fluorescence intensity in the nuclei of xenograft tumor tissues was significantly increased after sorcin knockdown (Fig. 9K and L). Moreover, the PAX5 protein levels in the cytoplasm and nucleus were also analyzed by Western blotting. Nuclear PAX5 levels were significantly increased after sorcin knockdown and decreased after sorcin overexpression, whereas cytoplasmic PAX5 levels were significantly decreased after sorcin knockdown and increased after

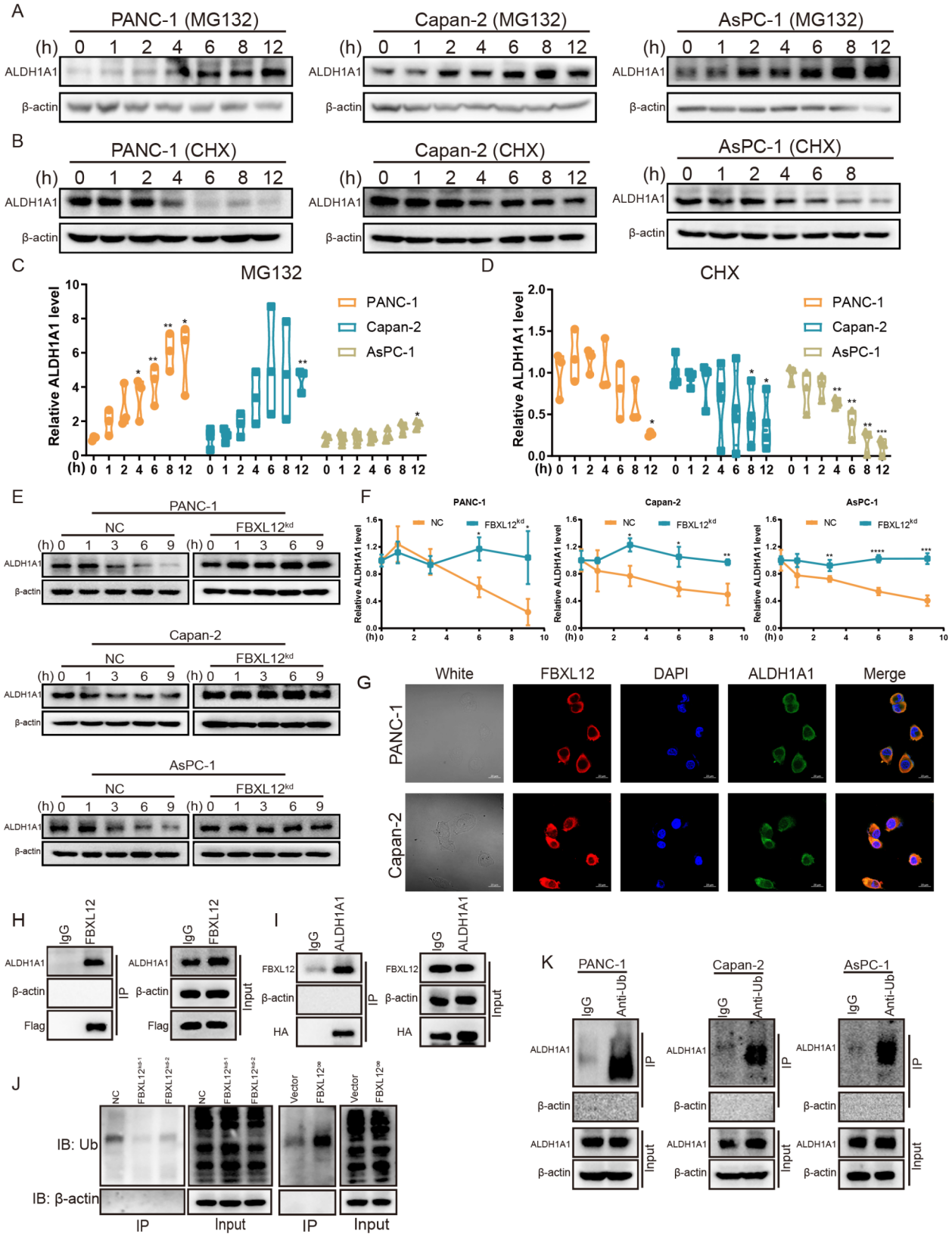

Fig. 8 (See legend on next page.)

(See figure on previous page.)

Fig. 8 FBXL12 mediated ALDH1A1 ubiquitination. (**A**) Western blotting analysis of ALDH1A1 protein levels in PANC-1, Capan-2 and AsPC-1 cells after treatment with MG132 at 10 μM for the indicated times. (**B**) Western blotting analysis of ALDH1A1 protein levels in PANC-1, Capan-2 and AsPC-1 cells after treatment with the protein synthesis inhibitor cycloheximide at 10 μM for the indicated times. (**C**) Statistical analysis of ALDH1A1 protein levels in PANC-1, Capan-2 and AsPC-1 cells after treatment with MG132 at 10 μM for the indicated times. (**D**) Statistical analysis of ALDH1A1 protein levels in PANC-1, Capan-2 and AsPC-1 cells after treatment with CHX at 10 μM for the indicated times. (**E**) Western blotting analysis of ALDH1A1 protein levels in FBXL12-knockdown PANC-1, Capan-2 and AsPC-1 cells after treatment with CHX at 10 μM for the indicated times. (**F**) Statistical analysis of ALDH1A1 protein levels in shRNA-induced FBXL12-knockdown cells after treatment with CHX at 10 μM for the indicated times. (**G**) Immunofluorescence analysis of ALDH1A1 colocalization with FBXL12 in PANC-1 and Capan-2 cells. (**H**) Analysis of the interaction between FBXL12 and ALDH1A1 after transfection with the pCMV-Flag-FBXL12 vector by coimmunoprecipitation with an anti-Flag antibody followed by Western blotting analysis. (**I**) Analysis of the interaction between FBXL12 and ALDH1A1 after transfection with the pCMV-HA-ALDH1A1 vector by coimmunoprecipitation with an HA antibody followed by Western blotting analysis. (**J**) Analysis of ALDH1A1 ubiquitylation after FBXL12 knockdown or overexpression by coimmunoprecipitation. (**K**) Analysis of the ubiquitylation of ALDH1A1 by coimmunoprecipitation with an anti-ubiquitin antibody followed by Western blotting analysis with antibodies against the indicated proteins

sorcin overexpression (Fig. 9M). Immunofluorescence staining of pancreatic cancer cells demonstrated that sorcin knockdown promoted PAX5 nuclear translocation, whereas sorcin overexpression inhibited this process (Fig. 9N). These findings indicated that the expression of sorcin was negatively correlated with the nuclear translocation of PAX5. These results demonstrated that sorcin decreased FBXL12 transcription by reducing the nuclear translocation of PAX5.

Identification of celastrol as a natural product that bound to Sorcin

Our findings suggested that sorcin regulates ferroptosis by interacting with PAX5, thus regulating FBXL12 gene expression and ultimately inducing ALDH1A1 ubiquitination-mediated degradation; these results indicated that sorcin may be a promising target for searches focused on identifying novel ferroptosis inducers. As a result, we endeavored to discover novel agents that induce ferroptosis by binding to sorcin. An in-house screen of 304 natural products was performed via a SPR assay (Fig. 10A), which led to the identification of celastrol, which is a naturally occurring triterpenoid (Fig. 10B) and interacted most strongly with the sorcin protein (*Kd* value of 2.13 μM) (Fig. 10C). Next, we evaluated the cytotoxic effects of celastrol on different pancreatic cancer cells. The cytotoxicity results suggested that celastrol inhibited the proliferation of pancreatic cancer cells, including PANC-1, Capan-2, AsPC-1 and PaTu8988T cells, in a dose-dependent manner (Fig. 10D and E). A colony formation assay revealed that celastrol strongly decreased the number of colonies (Fig. 10F). Moreover, celastrol significantly inhibited the migration of the PANC-1, AsPC-1 and Capan-2 pancreatic cell lines (Fig. 10G). Temperature-dependent cellular thermal shift assays (CETSAs) demonstrated that celastrol increased the thermal stability of the sorcin protein when exposed to high temperature (Fig. 10H and I). Moreover, a CETSA performed with different doses of celastrol suggested that celastrol increased the stability of sorcin in a dose-dependent manner, indicating a direct interaction between sorcin and celastrol (Fig. 10H and J).

To further investigate whether celastrol directly and covalently bound to the sorcin protein in cells, we first designed and synthesized probe **2** (Fig. 10K), which has better anti-pancreatic cancer activity as celastrol (Fig. 10L). Probe **2** was used to perform an *in situ* click chemistry assay, and it could replace celastrol to tag the potential cellular target of celastrol in the native cellular environment. The in situ pull-down experiment further indicated that sorcin was directly pulled down by probe **2**, which demonstrated that celastrol directly bound to sorcin intracellularly (Fig. 10M and N). Moreover, biotin-conjugated probe **4** was synthesized to further verify the binding effect *in vitro* (Fig. 10K). Pancreatic cancer cell lysates were incubated with probe **4** at different concentrations. Then, probe **4** was removed, and the proteins were incubated with streptavidin–agarose beads overnight. After affinity purification, the proteins that were precipitated by the streptavidin–agarose beads were resolved, followed by Western blotting analysis (Fig. 10O). The results showed that sorcin was specifically pulled down by probe **4** in a dose-dependent manner, which further confirmed that celastrol directly targeted sorcin (Fig. 10P and Q). Furthermore, we purified the sorcin protein and incubated it with celastrol alone. The binding curve of sorcin and probe **4** indicated time-dependent saturation, which was consistent with an irreversible binding mechanism with a K*obs* value of 0.067/min (Fig. 10R). Celastrol bound to the sorcin protein in a dose-dependent manner, with a K*i* value of 1.12 μM (Fig. 10S). Moreover, the quinine methide triterpenoid of celastrol is a reactive Michael acceptor. We hypothesized that celastrol covalently binds to the sorcin protein and that some conserved cysteine residues in sorcin may be binding sites of celastrol. To elucidate the specific binding site of celastrol, molecular docking calculations were conducted. An online tool, namely, POCASA 1.1, was used to predict the potential binding sites of small molecules, and several candidates were identified. After an analysis, the site near Cys194 was chosen as the docking pocket (Fig. 10T). To construct the structure of the covalent docking complex involving sorcin and celastrol, the pose of 5MRA was selected as the basis of manual

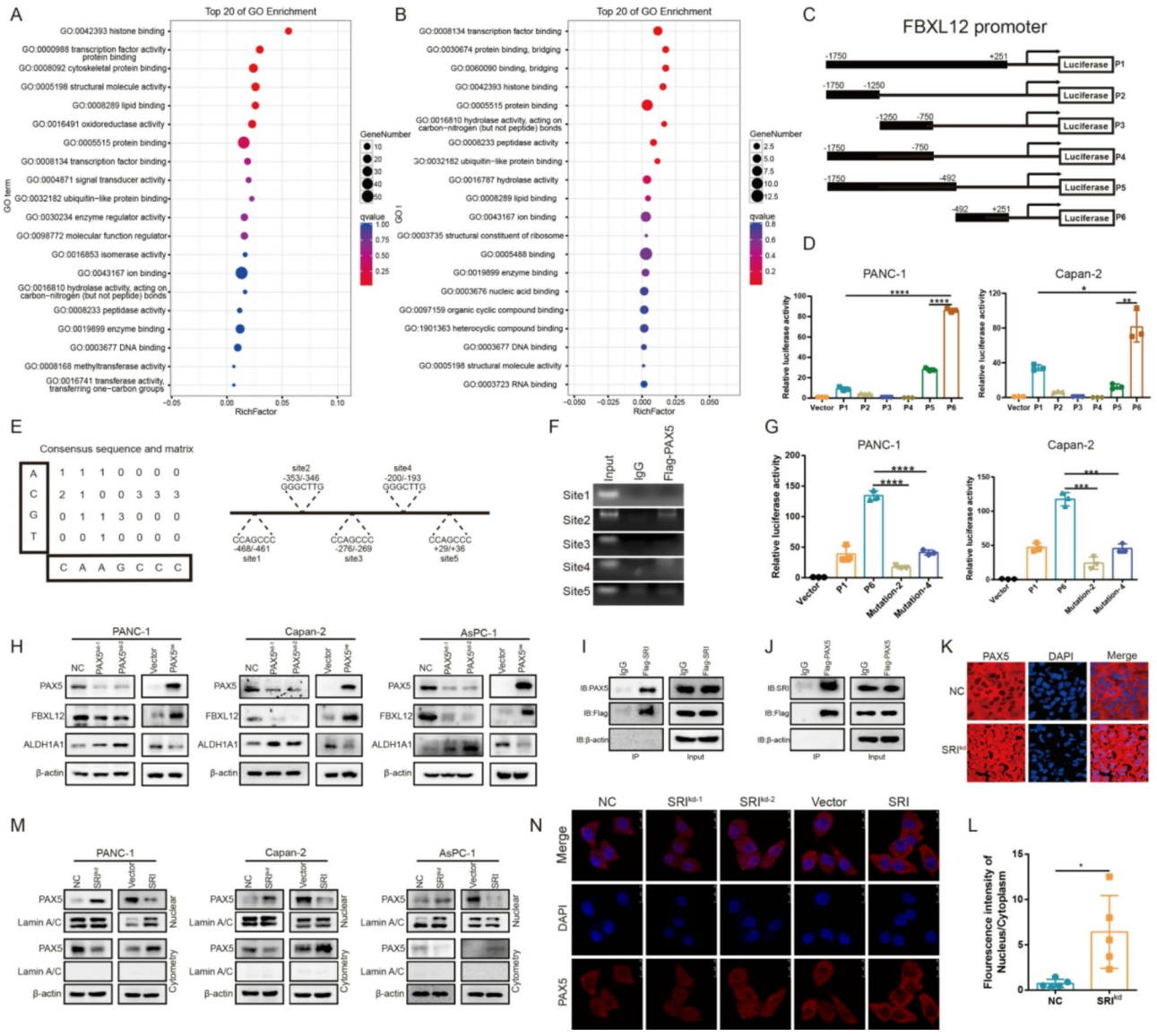

Fig. 9 Sorcin mediated the nuclear translocation of PAX5 to regulate FBXL12 transcription. (**A**) GO analysis of proteins whose expression significantly changed after sorcin was knocked down by shRNA according to the proteomics results. (**B**) GO proteomics analysis of proteins whose expression significantly changed after sorcin overexpression. (**C**) Schematic illustration of the cloned fragments in the human FBXL12 promoter. (**D**) Luciferase activity of the FBXL12 promoter fragments in PANC-1 and Capan-2 cells. (**E**) Base frequency rule and possible transcription factor-binding site analysis. (**F**) Ch-IP analysis of the five predicted PAX5 binding sites in the FBXL12 promoter sequence. IgG was used as a negative control. (**G**) Luciferase activity of the P6 promoter after mutation of site 2 or site 4 in PANC-1 and Capan-2 cells. (**H**) Western blotting analysis of PAX5, FBXL12 and ALDH1A1 expression in PANC-1, Capan-2 and AsPC-1 cells after PAX5 knockdown or overexpression. (**I**) Analysis of the interaction between PAX5 and sorcin after transfection with the pCMV-Flag-sorcin vector by coimmunoprecipitation with an anti-Flag antibody followed by Western blotting analysis. (**J**) Analysis of the interaction between PAX5 and sorcin after transfection with the pCMV-Flag-PAX5 vector by coimmunoprecipitation with an anti-Flag antibody followed by Western blotting analysis. (**K**) Immunofluorescence analysis of PAX5 nuclear translocation in sorcin-knockdown xenograft tumor tissues. (**L**) Statistical analysis of the immunofluorescence intensity of PAX5 nuclear translocation in sorcin-knockdown xenograft tumor tissues. (**M**) Western blotting analysis of PAX5 expression in the nucleus and cytoplasm of PANC-1, AsPC-1 and Capan-2 cells after sorcin knockdown and overexpression. (**N**) Immunofluorescence analysis of PAX5 levels in the nucleus and cytoplasm in PANC-1 cells after sorcin knockdown and overexpression

connection between the double-bonded carbon atom and the sulfur atom of Cys194 and subsequent energy minimization. As a result, we proposed (with the aid of computer docking) that cysteine 194, which is located in the pocket of sorcin, would be the main binding site of celastrol (Fig. 10T). To verify this hypothesis, we mutated cysteine 194 in sorcin to serine. The wild-type Cys194 mutant sorcin proteins were subsequently purified, incubated with probe **4** to perform a pull-down assay, and detected by Western blotting. The results indicated that

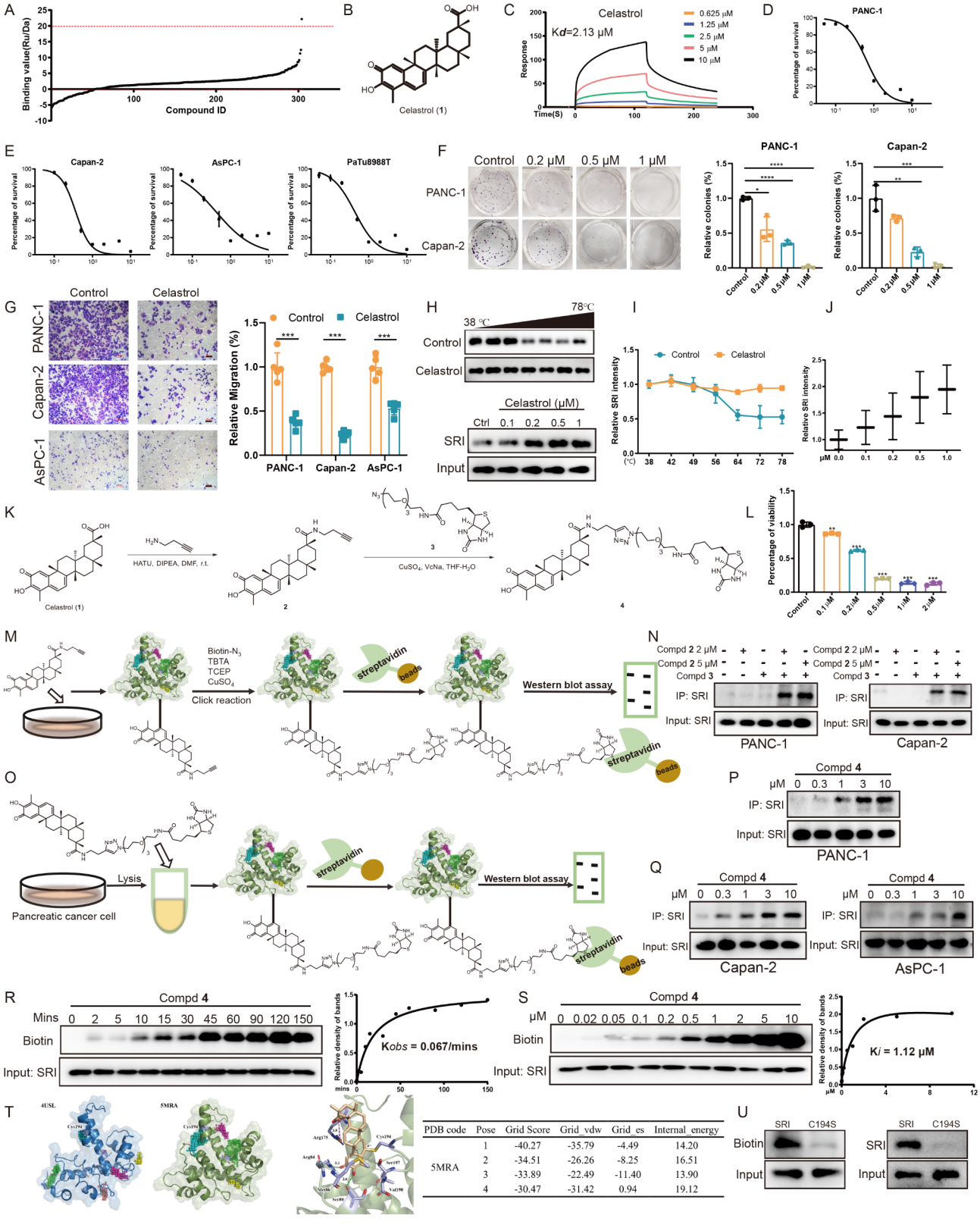

Fig. 10 Identification of celastrol as a natural product that bound to sorcin

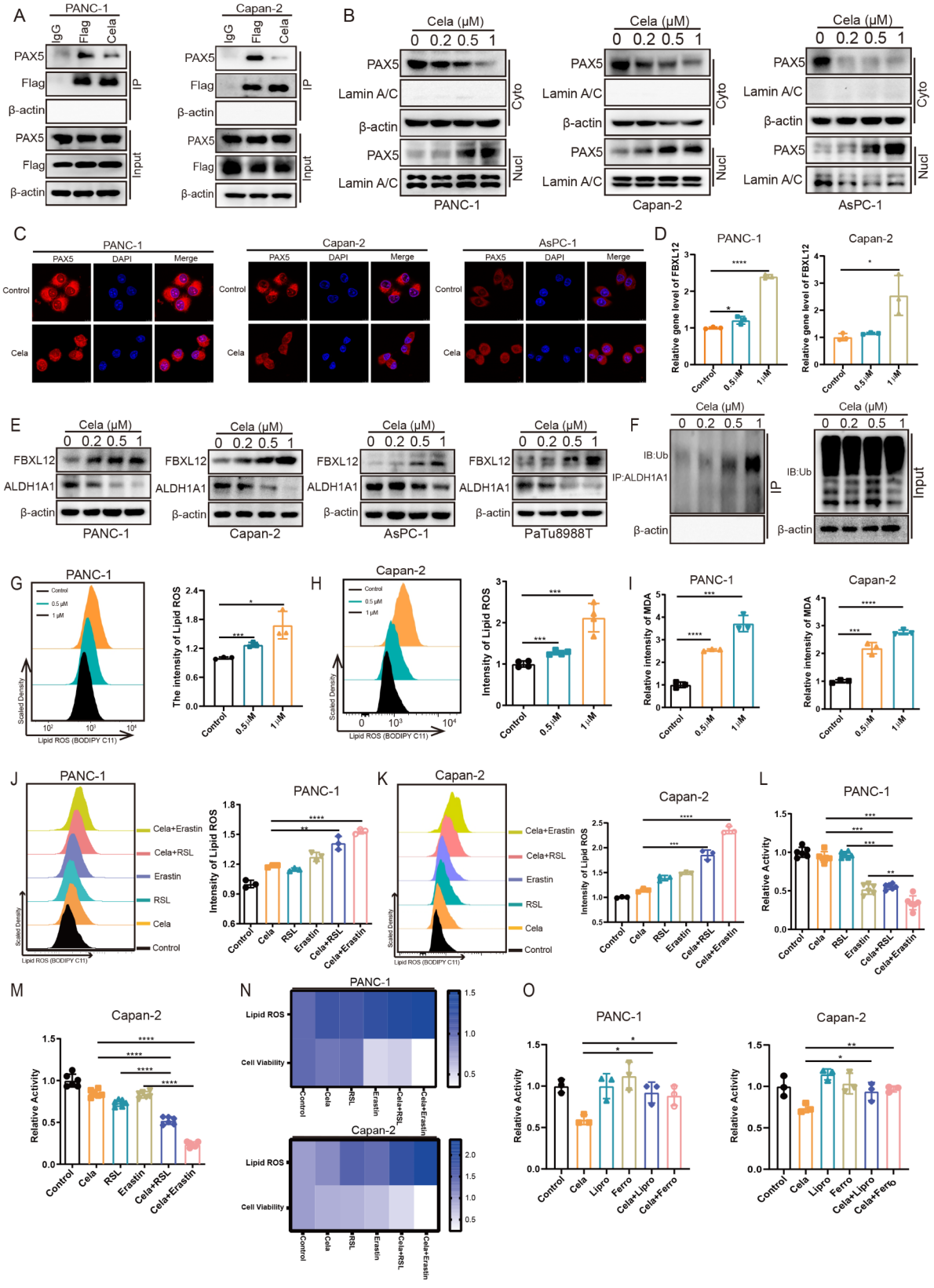

Fig. 11 (See legend on next page.)

(See figure on previous page.)

Fig. 11 Celastrol induced ferroptosis by promoting the nuclear translocation of PAX5. (**A**)Coimmunoprecipitation analysis of the interaction between PAX5 and sorcin after treatment with celastrol for 48 h. (**B**) Western blotting analysis of PAX5 levels in the nucleus and cytoplasm of PANC-1, Capan-2 and AsPC-1 cells after treatment with the indicated concentrations of celastrol for 48 h. (**C**) Immunofluorescence analysis of PAX5 levels in the nucleus and cytoplasm after treatment with celastrol for 48 h. (**D**) Quantitative analysis of FBXL12 gene expression after treatment with the indicated concentrations of celastrol for 24 h. (**E**) Western blotting analysis of FBXL12 and ALDH1A1 expression in PANC-1, Capan-2, AsPC-1 and PaTu8988T cells after treatment with celastrol at the indicated concentrations for 48 h. (**F**) Coimmunoprecipitation analysis of ALDH1A1 ubiquitylation after treatment with the indicated concentrations of celastrol for 48 h. (**G**) Representative images and statistical analysis of lipid ROS levels in PANC-1 cells after treatment with the indicated concentrations of celastrol for 48 h. (**H**) Representative images and statistical analysis of lipid ROS levels in Capan-2 cells after treatment with the indicated concentrations of celastrol for 48 h. (**I**) Analysis of malondialdehyde levels after treatment with the indicated concentrations of celastrol for 48 h. (**J**) Representative images and statistical analysis of lipid ROS levels in PANC-1 cells treated with celastrol combined with RSL3 (1 μM) or erastin (2 μM). (**K**) Representative images and statistical analysis of lipid ROS levels in Capan-2 cells treated with celastrol combined with RSL3 (1 μM) or erastin (1 μM). (**L**) Analysis of the viability of the indicated PANC-1 cells treated with celastrol combined with RSL3 or erastin. (**M**) Analysis of the viability of the indicated Capan-2 cells treated with celastrol combined with RSL3 or erastin. (**N**) Comparison of the cell viability and lipid ROS levels of the indicated cells. (**O**) Analysis of the viability of the indicated cells treated with celastrol combined with liproxstatin-1 or ferrostatin-1.

the amount of the sorcin protein that was pulled down by probe **4** was significantly reduced after cysteine 194 was mutated (Fig. 10U), which suggested that Cys194 of sorcin was critical for the covalent binding of celastrol.

Celastrol induced ferroptosis by promoting the nuclear translocation of PAX5

Our mechanistic research demonstrated that sorcin interacted with PAX5, inhibiting the nuclear translocation of PAX5, thereby decreasing FBXL12 transcription, and eventually increasing ALDH1A1 protein levels to suppress ferroptosis. However, whether celastrol, which is a specific interacting partner of sorcin, affects the interaction between sorcin and PAX5 and induces ferroptosis needed to be investigated. A coimmunoprecipitation assay revealed that celastrol disrupted the interaction between sorcin and PAX5 in pancreatic cancer cells by directly targeting sorcin (Fig. 11A). Then, we detected the nuclear translocation of PAX5 by Western blotting and immunofluorescence assays. The results revealed that the nuclear PAX5 protein levels were significantly increased, whereas the cytoplasmic PAX5 protein levels were significantly decreased after celastrol treatment (Fig. 11B). The fluorescence intensity of PAX5 in the nucleus was significantly increased, whereas that in the cytoplasm was decreased after celastrol treatment (Fig. 11C). These results confirmed that celastrol promoted the nuclear translocation of PAX5 by disrupting its interaction with sorcin. Moreover, FBXL12 gene expression and protein expression were obviously increased, whereas ALDH1A1 protein expression was significantly decreased by celastrol treatment in a dose-dependent manner (Fig. 11D and E). A coimmunoprecipitation assay with an anti-ALDH1A1 antibody revealed that the ubiquitylation of ALDH1A1 was distinctly increased after celastrol treatment (Fig. 11F).

Furthermore, flow cytometry revealed that celastrol increased the lipid peroxidation levels and malondialdehyde contents in pancreatic cancer cells, indicating that celastrol induced pancreatic cancer cell ferroptosis (Fig. 11G and I). To further validate the ability of celastrol to promote ferroptosis, lipid ROS levels and cell viability were measured in response to the combination of celastrol and ferroptosis inducers. The results demonstrated that celastrol markedly amplified the accumulation of lipid ROS induced by RSL3 and erastin (Fig. 11J and K). Additionally, celastrol obviously promoted the cytotoxic effects of RSL3 and erastin (Fig. 11L and M). Moreover, the results also revealed that lipid ROS levels were negatively correlated with cell viability after celastrol treatment (Fig. 11N). We further analyzed the combined effects of ferroptosis inhibitors and celastrol. The results indicated that ferroptosis inhibitors, including liproxstatin-1 and ferrostatin-1, could counteract the effect of celastrol, which suggested that celastrol induced ferroptosis in pancreatic cancer cells (Fig. 11O).

Celastrol inhibited tumor growth in CDX and PDX mouse models

We further investigated the effect of celastrol *in vivo* in a cell-derived mouse xenograft (CDX) tumor model and a patient-derived xenograft (PDX) model. The CDX model results showed that celastrol clearly decreased the pancreatic tumor volume and tumor weight *in vivo* (Fig. 12A and D). The PDX model results also confirmed that celastrol inhibited patient-derived tumor volume and weight *in vivo* (Fig. 12F and I). Moreover, the IHC assay results clearly revealed that the ALDH1A1 levels were reduced, whereas the FBXL12 levels were increased after celastrol administration (Fig. 12E and J).

On the basis of these studies, we proposed a mechanism underlying the effects of celastrol: celastrol first binds to sorcin and disrupts the interaction between sorcin and PAX5. This promotes of nuclear translocation of PAX5, induces the expression of FBXL12, and then increases the ubiquitylation of ALDH1A1, eventually inducing pancreatic cancer cell ferroptosis (Fig. 13).

Discussion

Pancreatic cancer has the worst prognosis and the highest mortality rate. Ferroptosis plays a crucial role in tumor progression, providing a new therapeutic strategy

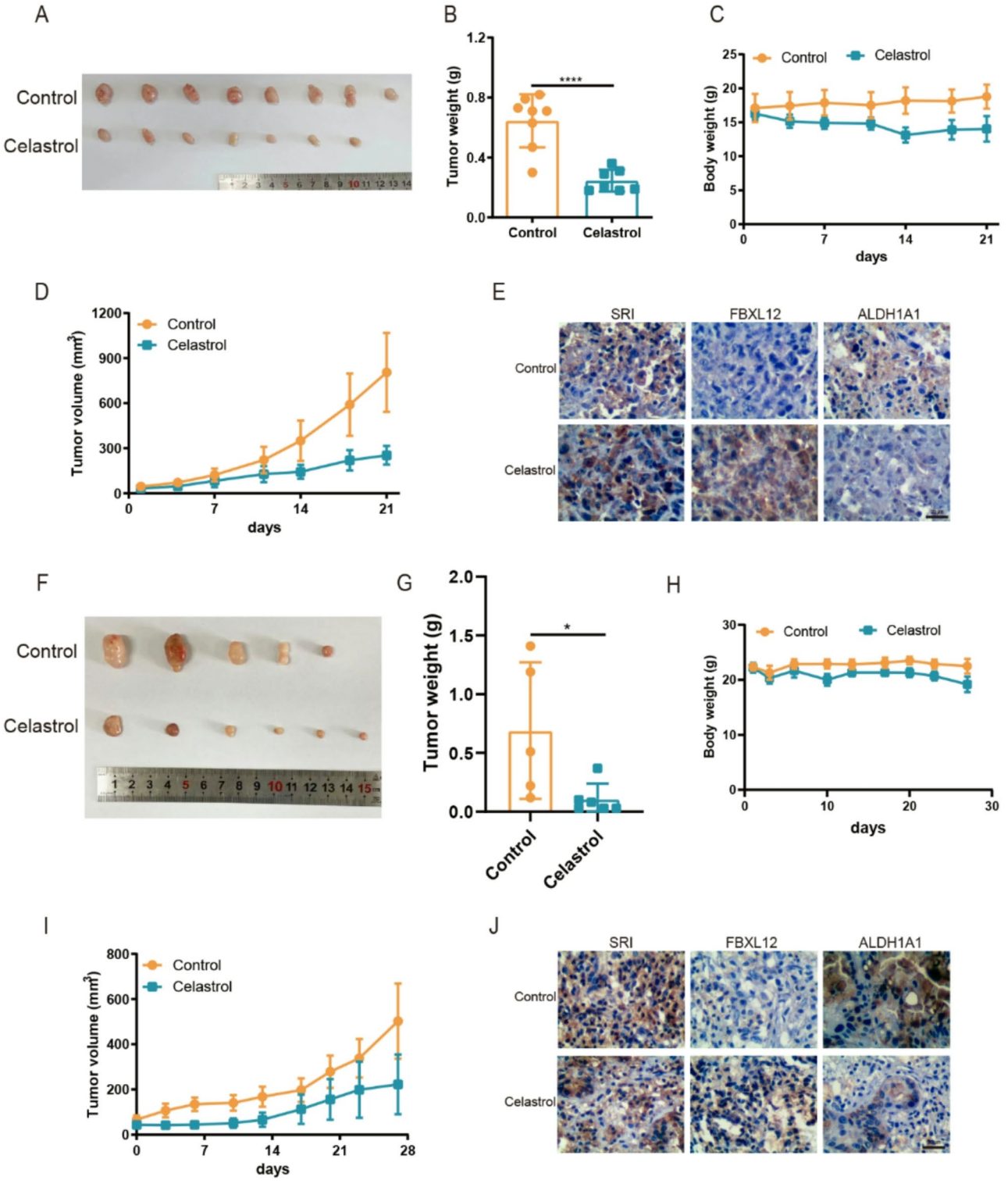

Fig. 12 Celastrol inhibited tumor growth in CDX and PDX mouse models. (**A**) Images of tumors from mice engrafted with PANC-1 cells after the intraperitoneal administration of celastrol (5 mg/kg). (B-D) Tumor weight, body weight and tumor volume after the administration of celastrol (5 mg/kg). (**E**) IHC analysis of the sorcin, FBXL12 and ALDH1A1 protein levels in a xenograft tumor model after the administration of celastrol. (**F**) Images of tumors from PDX model mice after the intraperitoneal administration of celastrol (5 mg/kg). (**G**-**I**) Tumor weight, body weight and tumor volume after the administration of celastrol to the PDX model (5 mg/kg). (**J**) IHC analysis of the sorcin, FBXL12 and ALDH1A1 protein levels in the PDX tumor model after the administration of celastrol

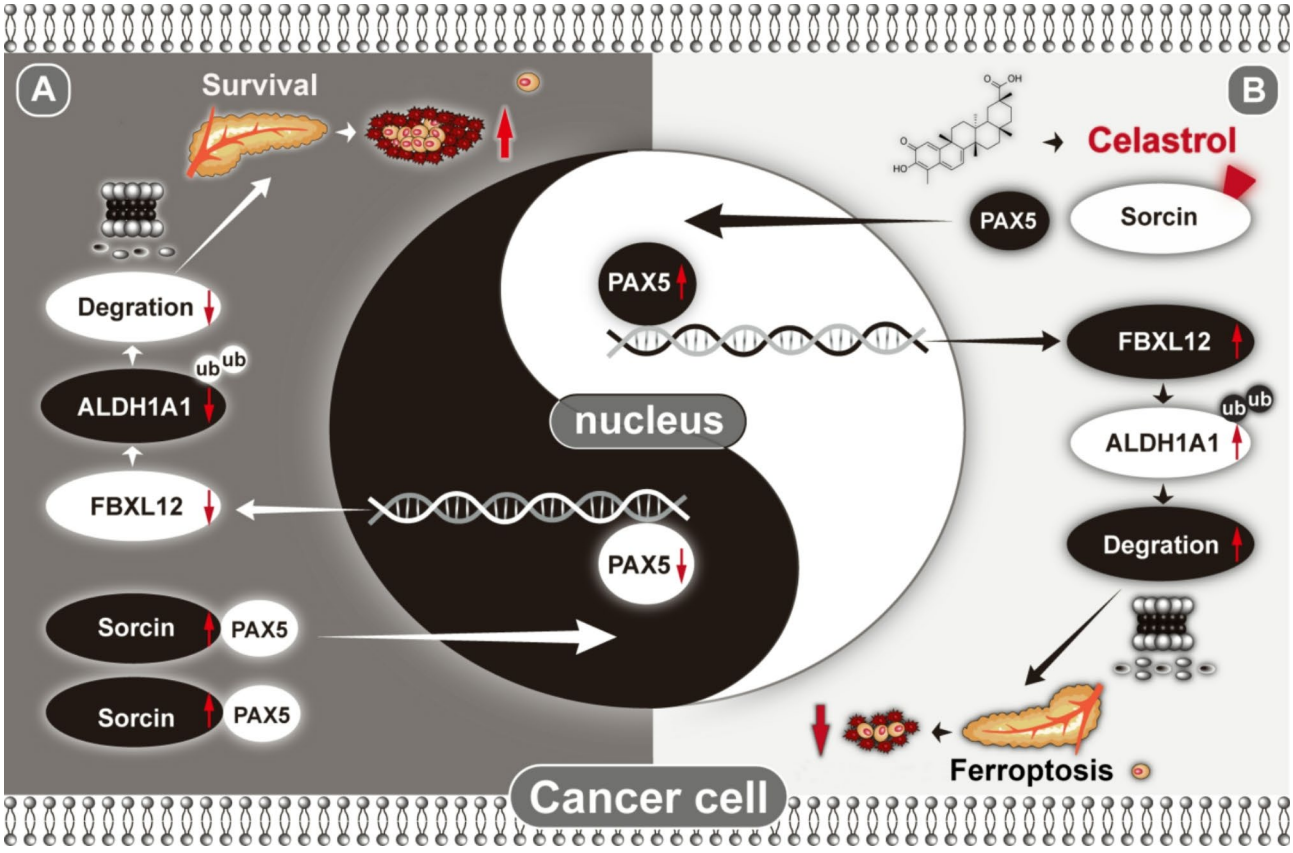

Fig. 13 Schematic diagram of our proposed model of the mechanism by which elevated sorcin suppresses ferroptosis and by which celastrol induced ferroptosis in pancreatic cancer cells

for treating cancer [43]. Extensive studies have indicated that the induction of ferroptosis reverses resistance to chemotherapy and acquired resistance to targeted therapy by regulating the canonical GPX4-dependent pathway and the noncanonical GPX4-independent pathway [44]. Sorcin, which is also called soluble resistance-related calcium binding protein, has been shown to play important roles in cancer progression, including roles in tumorigenesis, apoptosis, metastasis, and multidrug resistance, by regulating important proteins that are associated with the process of carcinogenesis [35, 36, 38]. Moreover, inhibiting sorcin expression reverses MDR [45]. However, the exact mechanism underlying the function of sorcin remains unclear. In this study, we first confirmed that sorcin was overexpressed in pancreatic cancer tissues compared with normal tissues and that it may represent a novel prognostic index for predicting the progression of pancreatic cancer or the overall survival of patients with pancreatic cancer; these results indicated that sorcin is a fascinating target for cancer therapy. Moreover, we discovered that sorcin knockdown promoted pancreatic cancer cell ferroptosis by inhibiting ALDH1A1 expression, suggesting that sorcin was also a prominent target for regulating ferroptosis.

Sorcin participates in the regulation of calcium homeostasis by binding to calcium. Moreover, sorcin can inhibit the ryanodine receptor and upregulate sarco (endo) plasmic reticulum Ca^{2+} ATPase (SERCA), which leads to increased calcium accumulation in the endoplasmic reticulum [46]. Therefore, we predicted that the knockdown of sorcin would increase the level of intracellular free calcium. Our experiments demonstrated that the knockdown of sorcin increased the concentration of Ca^{2+} in pancreatic cancer cells. As reported, increased intracellular Ca^{2+} levels result in increased ROS production, which induces ferroptosis. However, in this study, we discovered that sorcin regulated ALDH1A1 levels in a Ca^{2+}-independent manner to induce ferroptosis. Members of the aldehyde dehydrogenase (ALDH) family, which is a family of intracellular enzymes that consists of 19 isozymes with various substrates, were identified as being biomarkers of cancer stem-like cells in various types of tumors [47]. Moreover, ALDH1s play important roles in tumorigenicity, cancer metastasis and drug detoxification because of their unique enzyme function that oxidizes aldehydes to their corresponding acids [32, 48]. In particular, ALDH1s contribute to therapeutic resistance and are involved in the detoxification of aldehydes that

are produced by lipid peroxidation, which is the executor of ferroptosis [49]. Xin Chen and colleagues reported that ALDH1B1 suppressed 4HNE (4-hydroxynonenal)-mediated ferroptosis by blocking 4HNE-triggered lipid peroxidation [50]. Yang Wu and colleagues reported that ALDH1A3 expression was correlated with RSL3-induced ferroptosis, which suggested that ALDH1A3 expression regulated ferroptosis [51]. However, the function of ALDH1A1, which is the main ALDH1 activation component [52], in ferroptosis is still needed to be further investigated. In this study, we demonstrated that ALDH1A1 inhibited ferroptosis and that ALDH1A1 knockdown significantly promoted ferroptosis by increasing MDA levels.

Next, we discovered that sorcin regulated ALDH1A1 protein levels by increasing FBXL12 gene expression. FBXL12 is a ubiquitin E3 ligase. It has been reported that FBXL12 increases p21 expression levels via interaction, regulates the ubiquitination-mediated degradation of ALDH3 during placental development, induces G1 arrest by mediating the degradation of calmodulin kinase I, participate in DNA damage by inducing Ku80 ubiquitylation, and targets CDNK1B for polyubiquitylation and proteasomal degradation [53–56]. However, FBXL12 has not attracted sufficient attention, and its substrate has rarely been reported. Herein, we revealed that FBXL12 induced the ubiquitination and degradation of ALDH1A1, which suggested that ALDH1A1 was the substrate of FBXL12; however, the type of ubiquitination of ALDH1A1 should be identified in future work. Moreover, the regulatory mechanism of FBXL12 is still unclear. In this study, we confirmed that PAX5 regulated FBXL12 gene transcription. PAX5, which is a B cell-specific transcription factor, plays an important activating role during B lymphoid cell differentiation and neural development [57]. PAX5 serves as a marker of progression in B cell cancers, lung cancer, neuroblastoma and cervical carcinoma and is used for cancer diagnosis and monitoring of treatment efficacy [58]. In contrast to its oncogenic effects in B cell cancers, PAX5 is considered a tumor suppressor in some carcinomas, including hepatocellular carcinoma, esophageal squamous cell carcinoma and gastric cancer [58]. PAX5-knockdown cells exhibit significantly increased cell proliferation and cisplatin resistance. Moreover, methylation of PAX5 was shown to be an extremely tumor-specific event in squamous cell carcinogenesis of the head and neck [59]. However, despite the ubiquitous expression of PAX5 in different tissues, the mechanisms that are responsible for its opposite effects on different cancers are not fully understood. Our research indicated that PAX5 mediated FBXL12 transcription to regulate ALDH1A1 levels. A mechanistic study demonstrated that when overexpressed, the sorcin protein interacted with PAX5 in the cytoplasm and inhibited the nuclear translocation of PAX5, thus inhibiting FBXL12 transcription. These upstream and downstream mechanisms provide new insights into the function of PAX5, and regulating PAX5 nuclear translocation might be important for cancer treatment.

Natural products have been explored as invaluable sources for drug discovery [60]. For example, parthenolide, which is an active component, selectively eliminates leukemia stem cells [61]. We developed the derivative DMAMCL (registered as ACT001), which has currently completed a phase I trial in Australia (ID: ACTRN12616000228482), developed phase II clinical trials for glioblastoma therapy in China (ID: 2020LP00423) and phase 1b/2a clinical trials in patients with surgically accessible recurrent glioblastoma multiforme in America (ID: NCT05053880), and this agent has been granted orphan drug status by the FDA and EMA. The clinical results of ACT001 encouraged us to further identify natural products for clinical use. The discovery of drugs from natural product sources on the basis of new mechanisms is very important, especially when structural modifications can be introduced to reduce toxicity and increase activity. We screened an in-house collection of 304 natural products via an SPR-based assay to identify a product that strongly binds to sorcin. Celastrol, which is a naturally occurring quinine methide triterpenoid that is isolated from the root of *Tripterygium wilfordii*, was identified as a product that strongly binds to sorcin. Celastrol has attracted increasing interest, especially because of its potent anticancer effects against numerous cancer cell lines. Several mechanisms underlying its effects, such as mechanisms that include Hsp90, NF-κB, Cdc37, and ATF2, have been identified [62]. In addition, during spinal cord injury recovery, celastrol acts as a ferroptosis inhibitor to inhibit oligodendrocyte and neuron ferroptosis [63]; acute kidney injury, celastrol alleviates ferroptosis through the Nrf2/GPX4 pathway [64]; and in liver fibrosis, celastrol induces ferroptosis in activated hepatic stellate cells [65].

Celastrol was suggested to undergo a conjugate addition of cysteine residues to its quinone methide substructure, and this interaction appeared to be crucial for its numerous biological properties [66, 67]. However, the exact mechanism still needed to be investigated. Our results suggested that celastrol could directly bind to sorcin and undergo Michael addition to the 194-cysteine residue of sorcin to induce ferroptosis. Further mechanistic studies revealed that celastrol increased FBXL12 protein levels by promoting PAX5 nuclear translocation. However, further clinical application of celastrol is limited because of its severe side effects. The findings of this study provide guidance for the further modification or improvement of celastrol and the identification of other novel ferroptosis-inducing drugs.

Collectively, our results demonstrated that sorcin was overexpressed in pancreatic cancer patient tissues, and that its expression was correlated with histological grade and overall survival. A mechanistic study revealed that when overexpressed, sorcin interacted with PAX5 in the cytoplasm, inhibited the nuclear translocation of PAX5, reduced the expression of FBXL12, decreased the ubiquitylation of ALDH1A1, and eventually suppressed ferroptosis in pancreatic cancer cells. Naturally occurring celastrol inhibited the interaction of sorcin with PAX5 by directly binding to the Cys194 residue of the sorcin protein, thus promoting the nuclear translocation of PAX5, inducing the expression of FBXL12, increasing the ubiquitylation of ALDH1A1, and eventually inducing pancreatic cancer cell ferroptosis (Fig. 13). Celastrol could be a natural lead compound for the development of ferroptosis-based drugs. These findings suggested that disrupting the sorcin–PAX5 interaction might be a promising therapeutic strategy for treating cancer by inducing ferroptosis.

Materials and methods

Cell culture and reagents

Human pancreatic cancer cell lines, including the PANC-1, AsPC-1, and PaTu8988T cell lines, were purchased (Fung Hui Biotechnology, China) and cultured in DMEM supplemented with 10% FBS at 37 °C in 5% CO_2. Capan-2 and MIA Paca-2 cells were obtained (ATCC, USA) and cultured in 1640 medium supplemented with 10% FBS at 37 °C in 5% CO_2. Specific antibodies against sorcin (ab71983) and FBXL12 (ab96831) were purchased from Abcam (Abcam, UK). Antibodies against ALDH1A1 (54135, D9Q8E), PAX5 (8970, D19F8), and Flag (8146, 9A3) were purchased from CST (Cell Signaling Technology, USA), and an antibody against β-actin (AF7018) was purchased from Affinity (Affinity Biosciences, USA).

IHC assay

The study of tissue samples from human subjects was approved by the Nankai University Ethical Committee. Human pancreatic cancer tissue chips (Shanghai Outdo Biotech Co., Ltd. and Xi'an Alina Bio-technology Co., Ltd) or animal tissue slides were deparaffinized with xylene and a series of gradient ethanol solutions. After antigen retrieval with EDTA, the slides were incubated with 3% H_2O_2 to block endogenous peroxidase activity. After 10 min, the slides were incubated with sheep serum, then incubated with primary antibodies overnight at 4 °C, and subsequently incubated with secondary antibodies. For the human pancreatic cancer tissue chips, the results were assessed according to the German semiquantitative scoring system: degree of staining: none (0), weak brown (1+), moderate brown (2+), and strong brown (3+). The samples were divided into 5 groups according to the percentage of stained tumor cells: 0 for no positive cells, 1 for 1–25% positive cells, 2 for 25–50% positive cells, 3 for 50–75% positive cells, and 4 for >75% positive cells. Multiplication of the intensity and percentage scores was used to determine the results (staining index). For the animal tissue slides or part of the human pancreatic cancer tissue chips, the intensity of the brown color was calculated by ImageJ.

Animal assay

The animal experiments were approved by the Nankai University Ethical Committee and conformed to the legal mandates and national guidelines for the care and maintenance of laboratory animals (2023-SYDWLL-000518). Five-week-old female BALB/c nude mice were purchased from Beijing Vital River Laboratory Animal Technology Co., Ltd. Briefly, PANC-1 cells (5×10^6) were subcutaneously injected into the armpit of the right forelimb. When tumor formation occurred, the tumor sizes were measured twice a week. The mice were sacrificed, and the tumor tissues were removed, sectioned, and analyzed by immunohistochemistry or immunofluorescence.

To evaluate the effect of celastrol, five-week-old female BALB/c nude mice were purchased from Beijing Vital River Laboratory Animal Technology Co., Ltd. Briefly, PANC-1 cells (5×10^6) were subcutaneously injected into the armpit of the right forelimb. After 6 weeks, the tumors were cut into small pieces and subcutaneously transplanted into new mice. When the tumor sizes reached 50–100 mm^3, celastrol (5 mg/kg) was administered by intraperitoneal injection. For patient-derived tumor xenografts (PDXs), mice bearing pancreatic cancer patient-derived tumor xenografts were purchased from Beijing IDMO Co., Ltd. After the tumors in the PDX model mice reached 500–1000 mm^3, the patient-derived tumors were removed, divided, and transplanted into BALB/c nude mice. Celastrol (5 mg/kg) was administered intraperitoneally, and the tumor volume was calculated.

Lentiviral transduction, vector, and SiRNA transfection

Pancreatic cancer cell lines were transfected with lentiviral particles for 48 h, after which puromycin (10 μg/mL) was added for selection. After 7 days of selection, the transfection efficiency was determined by Western blotting. The transfection of plasmids or siRNAs was conducted with Lipofectamine 3000 reagent according to the manufacturer's protocol.

Surface plasmon resonance (SPR) assay

The SPR experiment was performed with a Biacore T200. The sorcin protein (1 mg/mL) was immobilized via amine coupling onto a COOH5 sensor chip. The amount of immobilized sorcin reached 5000 response units (RUs). Our in-house natural products were dissolved in DMSO,

and the storage concentration was 20 mM. The compounds were diluted with PBS and were added to the assay with a contact time of 60 s, a dissociation time of 60 s, and a flow rate of 30 μL/min. The increase in RUs relative to the baseline value indicated the binding intensity between the immobilized sorcin ligand and each compound.

MTT assay

Pancreatic cancer cells in the logarithmic phase of growth were seeded in 96-well plates. After 6–8 h, the test compound was added at different concentrations and incubated for 72 h. After that, 20 μL of MTT solution (5 mg/mL) was added, and the sample was incubated for an additional 4 h. The supernatant was subsequently discarded, and the precipitate was dissolved in DMSO. The OD at 570 nm was measured, and the IC_{50} was calculated by GraphPad Prism.

Western blotting analysis

The cells were lysed with cell lysis buffer, and protein concentrations were quantified with a BCA protein assay kit. Proteins were resolved via 12% SDS–PAGE and transferred to polyvinylidene difluoride (PVDF) membranes, and then, the membranes were blocked with blocking solution (5% nonfat milk) for 1 h. The primary antibodies were diluted and incubated overnight at 4 °C. After being washed with PBST 5 times, the membranes were incubated with a horseradish peroxidase-conjugated secondary antibody for 3 h at room temperature. After washing with PBST 5 times, the bands were visualized using enhanced chemiluminescence luminescence and imaged with an ECL system.

Migration and invasion assays

Migration and invasion assays were performed in 24-well plates with 8-μm chambers. For the migration assays, 5×10^4 pancreatic cancer cells in FBS-free medium were plated in the upper chamber of the Transwell plate, and 700 μL of medium supplemented with 20% FBS was added to the lower chamber. After 24 h, the cells that had crossed through the filter membrane and entered the lower chamber were fixed in 4% paraformaldehyde and stained with crystal violet for 20 min at 4°C. For the invasion assay, the chambers were pretreated with Matrigel for 30 min at 37 °C. The remaining experimental procedures were the same as those in the migration assay.

ALDH assay

The ALDH assay was conducted with the ALDEFLUOR™ kit following the manufacturer's instructions (01700, STEMCELL Technologies). Pancreatic cancer cells were collected and washed with PBS 3 times. The cells were subsequently resuspended in 500 μL of assay buffer. After that, 2.5 μL of Aldefluor substrate was added and incubated for 60 min at 37 °C. The cells were treated with 2.5 μL of Aldefluor substrate and 5 μL of the ALDH inhibitor diethylamino-benzaldehyde (DEAB) as a negative control. After incubation, the cells were collected, washed, and analyzed by flow cytometry within 1 h.

BODIPY staining to assess lipid peroxidation

After treatment, pancreatic cancer cells were collected and washed with PBS. The cells were subsequently stained with BODIPY 581/591 C11 (5 μM) for 1 h at 37 °C. After washing with PBS, the fluorescence intensity was measured by FACS.

Nuclear and cytoplasmic protein extraction

After treatment, pancreatic cancer cells were collected and washed with PBS. Then, the nuclear proteins and cytoplasmic proteins were extracted according to the manufacturer's instructions (Beyotime, China).

Recombinant sorcin protein expression and purification

DNA sequences encoding the wild-type and Cys194 mutant sorcin proteins were inserted into the pET-28a vector plasmid. These plasmids were subsequently transformed into *Escherichia coli* cells. The *E. coli* cells were incubated at 37 °C in LB medium at 220 rpm/min until the OD_{600} reached 0.6–0.8. After that, IPTG was added at a final concentration of 500 μM, and protein expression was induced for another 16–18 h at 16 °C. The bacterial cells were subsequently collected and lysed with lysis buffer. After centrifugation, the supernatant was collected and incubated with Ni Sepharose beads. After washing with washing buffer to remove nonspecific binding proteins, the recombinant sorcin proteins were removed from the beads with elution buffer. The protein mixture was aliquoted and stored at -80 °C.

DIA proteomics

PANC-1 cells were collected, washed, lysed with lysis buffer, and homogenized for 3 min with an ultrasonic homogenizer. After centrifugation at 4 °C, the proteins in the supernatant were collected. After digestion with sequence-grade modified trypsin, the proteins were labeled with an iTRAQ labeling kit according to the manufacturer's instructions. The digested protein products were subsequently dried, dissolved and fractionated using an SCX column via HPLC. The peptides were analyzed by on-line nanospray LC–MS/MS on an Orbitrap Fusion Lumos coupled to an EASYnLC 1200 system via a C18 analytical reverse-phase column. The experimental procedures and data analysis were performed by Gene Denovo Biotechnology Co. (Guangzhou, China). Differentially expressed proteins were identified by Q values

(FDRs) smaller than 0.05 and absolute AVG $\log_2$ ratios greater than 0.58 according to Student's t test.

Calcium ion assay

Pancreatic cancer cells were collected, washed with PBS, and incubated with Fluo-3 AM (1 μM) at 37 °C for 1 h. The cells were subsequently washed with PBS buffer and incubated for another 30 min before flow cytometry was performed.

Bioinformatics analysis with the TCGA and GEO databases

The gene expression data of PAAD samples in the TCGA database were downloaded. The clinical information and survival data of individual pancreatic cancer patients were obtained from the TCGA database and TCGA Pan-Cancer Clinical Data Resource [68]. The samples were subsequently divided into a high sorcin expression group and low sorcin expression group according to the expression level of the sorcin gene. Overall survival (OS), disease-free survival (DFS), progression-free interval (PFI), progression-free survival (PFS) and the recurrence-free interval (RFI) were analyzed. For bioinformatics analysis with the GEO database, the gene expression data of cancer and normal tissues were downloaded from the Gene Expression Omnibus (GEO) database (https://www.ncbi.nlm.nih.gov/gds/), and datasets, including the GSE15471, GSE62165, GSE62452, and GSE28735 datasets, were selected for sorcin expression analysis. The GSE15471 dataset included data from 39 normal tissues and 39 tumor tissues from patients with pancreatic ductal adenocarcinoma. The GSE62165 dataset included data from 13 nontumoral pancreatic tissue samples and 118 pancreatic tumor samples of different stages. The GSE62452 dataset included data from 61 adjacent pancreatic nontumors and 69 pancreatic tumors of different stages. The GSE28735 dataset included data from 45 nontumor tissues and 45 tumor tissues from patients with pancreatic ductal adenocarcinoma. The gene expression of sorcin in these datasets was subsequently analyzed.

Cellular thermal shift assay

The recombinant sorcin protein was incubated with or without celastrol for 1 h at room temperature. The samples were subsequently heated at different temperatures (38–78 °C) for 3 min, followed by cooling at 4 °C. After centrifugation at 12,000 rpm for 15 min at 4 °C, the supernatant was collected, and the proteins were analyzed by Western blotting.

Transmission electron microscopy assay

The cells were cultured with 2×10^6 cells/dish, washed with PBS buffer, and fixed with 2.5% glutaraldehyde (pH 7.4). After washed 3 times with 0.1 M phosphate buffer (pH 7.2), the cells were treated with 1% osmic acid at 4 ℃ for 2 h. Then the samples were dehydrated with a graded series of ethanol, embedded in Epon-Araldite resin for penetration, and placed for polymerization. The ultrathin sections were made for microstructure analysis. After counterstaining with 3% uranyl acetate and 2.7% lead citrate, the sections was observed with transmission electron microscopy.

RNA extraction and qPCR assay

Pancreatic cancer cells were collected and lysed with TRIzol buffer. After chloroform extraction and isopropanol precipitation, total RNA was obtained and then reverse transcribed to cDNA with a cDNA synthesis kit. Then, quantitative PCR was performed, and the relative levels of the target genes were normalized to those of β-actin.

Tumorsphere assay

Pancreatic cancer cells were resuspended in MGM medium and mixed to obtain single-cell suspensions. These cells were then seeded in low-adhesion well plates. After approximately 7 days, the number of tumorspheres was counted under a microscope.

Coimmunoprecipitation analysis

Pancreatic cancer cells were transfected with the overexpression vector that included a Flag tag. After 48 h, the proteins were collected, and the indicated protein was immunoprecipitated from the cell lysates with an anti-Flag antibody. The immunocomplexes were collected with agarose, examined by Western blotting analysis and visualized via an ECL detection system.

Chromatin Immunoprecipitation assay

Pancreatic cancer cells were transfected with the p-CMV-Flag-PAX5 vector for 48 h. Then, the cells (2×10^6) were seeded in 10-cm diameter culture dishes and treated with 1% formaldehyde at 37 °C for 10 min to cross-link the proteins to the DNA. After the cross-linking was stopped with glycine, the cell lysates were sonicated to fragment the DNA into 200–1000-bp fragments. Then, an anti-Flag antibody (1 μg) was added, and the mixture was incubated at 4 °C overnight. After that, 60 μL of protein A + G agarose was added, and the mixture was incubated on a shaker for 60 min at room temperature. The protein A + G agarose was collected, and the free DNA was obtained by reversing the cross-linking of protein–DNA complexes. Real-time PCR was carried out to determine the quantity of DNA.

Luciferase reporter assay

PANC-1 and Capan-2 cells were seeded in 24-well plates at 5×10^4 cells/well. After 12 h, the cells were transfected with pGL3 basic plasmids (0.8 μg) and 50 ng of a pRL-TK

Renilla plasmid with Lipofectamine 2000 reagent for 24 h. The cells were lysed, and the luciferase and Renilla signals were determined 24 h after transfection using a Dual Luciferase Reporter Assay Kit (Vazyme, China).

Immunofluorescence assay

The tumor tissues were cut into frozen sections. Briefly, the slides were air-dried and fixed with ice-cold methanol for 10 min. Then, the slides were blocked with horse serum for 30 min at room temperature. After that, the slides were incubated with primary antibodies at 4 °C overnight. The slides were washed and incubated with fluorescent secondary antibodies for 1 h in the dark. The slides were washed with PBST 5 times, stained with DAPI for 10 min and visualized under a fluorescence microscope. The immunofluorescence assay for cultured cells followed a method similar to the method described above.

Molecular docking

Molecular docking calculations were conducted using the Dock6 protocol on the Yinfo Cloud Platform (http://cloud.yinfotek.com/). The chemical structure of celastrol (1) was drawn by JSME and converted to a 3D structure with energy minimization in the MMFF94 force field. The crystal structures (PDB code: 5MRA; resolution: 3.74 Å) of sorcin were automatically downloaded from the RCSB Protein Data Bank. All the redundant atoms except chain A were deleted, and then, the protein structures were carefully treated in several steps, including residue repair, protonation, and partial charge assignment, in the AMBER ff14SB force field. An online tool, namely, POCASA 1.1 (http://altair.sci.hokudai.ac.jp/g6/service/pocasa/), was used to predict the potential small molecule binding sites, and several candidates were identified. After analysis, the site near Cys194 was chosen as the docking pocket. The DMS tool was then used to build the molecular surface of the receptor using a probe atom with a 1.4 Å radius, and spheres were generated that filled the site from the Sphgen module in UCSF Chimera. A box enclosing the spheres was set with centers of (-2.033, 31.818, -21.074) and (-16.950, -16.308, 21.176) and sizes of (32.549, 29.130, 29.063) and (23.691, 21.781, 22.551). Within the pocket, the grids that were necessary for rapid score evaluation were created by the Grid module. Finally, the DOCK 6.7 program was utilized to conduct semiflexible docking where 10,000 different orientations were produced. Clustering analysis was performed (the RMSD threshold was set to 2.0 Å) for candidate poses, and the poses with the best scores were output. To construct the structure of the covalent docking complex involving sorcin and Compound 1, the pose of 5MRA was selected as the basis of manual connection between the double-bonded carbon atom and the sulfur atom of Cys194 and subsequent energy minimization.

Statistical analysis

All the data were analyzed using GraphPad Prism. The differences between groups were analyzed by Student's t test. The data are presented as the means ± SDs. The test results were considered statistically significant at $^{*}P<0.05$, $^{**}P<0.01$, $^{***}P<0.005$, and $^{****}P<0.001$.

Abbreviations

SRI	Sorcin
CESTA	Cellular thermal shift assays
MDR	Multidrug resistance
EMT	Epithelial-to-mesenchymal transition
CSC	Cancer stem cell
Ferro	Ferrostatin-1
Lipro	Liproxstatin-1
Cela	Celastrol
DSF	Disulfiram
DEAB	4-diethylaminobenzaldehyde
Compd	compound
MDA	Malondialdehyde
CSC	cancer stem cell
SPR	surface plasmon resonance
GEO	Gene Expression Omnibus
PLOOHs	phospholipid hydroperoxides
PDAC	Pancreatic ductal adenocarcinoma

Supplementary Information

The online version contains supplementary material available at https://doi.org/10.1186/s13045-025-01680-8.

Supplementary Material 1

Author contributions

Q.Z. and Y.D. designed research; Y.D., Y.B., T.C., S.C., W.F., and S.M. performed research; Q.Z. Y.D., Y.B., S.C., T.C., W.F., and S.M. analyzed data; Q.Z. and Y.D. wrote the paper.

Funding

This research was supported by the National Natural Science Foundation of China (NO. 82273808, 81872764 to Q.Z. and NO. 82272654, 81903456 to Y.D.).

Data availability

No datasets were generated or analysed during the current study.

Declarations

Ethical approval

The study was approved by the Ethics Committee of Nankai University (NKUIRB2023088) and conducted in accordance with the Declaration of Helsinki. And the animal experiments were approved by Nankai University Ethical Committee (2023-SYDWLL-000518) and conformed to the legal mandates and national guidelines for the care and maintenance of laboratory animals.

Competing interests

The authors declare no competing interests.

Author details

[1]State Key Laboratory of Medicinal Chemical Biology, College of Pharmacy and Tianjin Key Laboratory of Molecular Drug Research, Nankai University, Haihe Education Park, 38 Tongyan Road, Tianjin 300353, People's Republic of China

[2]College of Chemistry, Nankai University, 94 Weijin Road, Tianjin 300071, People's Republic of China
[3]College of Pharmacy, Nankai University, Haihe Education Park, 38 Tongyan Road, Tianjin 300353, People's Republic of China

Received: 28 May 2024 / Accepted: 24 February 2025
Published online: 07 March 2025

References

1. Hidalgo M. Pancreatic cancer. N Engl J Med. 2010;362:1605–17.
2. Siegel RL, Miller KD, Jemal A, Cancer, Statistics. 2017. CA Cancer J Clin 67, 7–30 (2017).
3. Siegel RL, Miller KD, Jemal A. Cancer statistics, 2018. CA Cancer J Clin. 2018;68:7–30.
4. Muniraj T, Jamidar PA, Aslanian HR. Pancreatic cancer: a comprehensive review and update. Dis Mon. 2013;59:368–402.
5. Pelosi E, Castelli G, Testa U. Pancreatic cancer: molecular characterization, clonal evolution and Cancer stem cells. Biomedicines 5 (2017).
6. Rahib L, et al. Projecting cancer incidence and deaths to 2030: the unexpected burden of thyroid, liver, and pancreas cancers in the united States. Cancer Res. 2014;74:2913–21.
7. Chen W. Cancer statistics: updated cancer burden in China. Chin J Cancer Res. 2015;27:1.
8. Weizman N, et al. Macrophages mediate gemcitabine resistance of pancreatic adenocarcinoma by upregulating cytidine deaminase. Oncogene. 2014;33:3812–9.
9. Garrido-Laguna I, Hidalgo M. Pancreatic cancer: from state-of-the-art treatments to promising novel therapies. Nat Rev Clin Oncol. 2015;12:319–34.
10. Ryan DP, Hong TS, Bardeesy N. Pancreatic adenocarcinoma. N Engl J Med. 2014;371:1039–49.
11. Huang ZQ, Saluja AK, Dudeja V, Vickers SM, Buchsbaum DJ. Molecular targeted approaches for treatment of pancreatic cancer. Curr Pharm Des. 2011;17:2221–38.
12. Dixon SJ, et al. Ferroptosis: an iron-dependent form of nonapoptotic cell death. Cell. 2012;149:1060–72.
13. Wang H, Liu C, Zhao Y, Gao G. Mitochondria regulation in ferroptosis. Eur J Cell Biol. 2020;99:151058.
14. von Krusenstiern AN, et al. Identification of essential sites of lipid peroxidation in ferroptosis. Nat Chem Biol. 2023;19:719–30.
15. Jiang X, Stockwell BR, Conrad M. Ferroptosis: mechanisms, biology and role in disease. Nat Rev Mol Cell Biol. 2021;22:266–82.
16. Yang WS, et al. Regulation of ferroptotic cancer cell death by GPX4. Cell. 2014;156:317–31.
17. Bersuker K, et al. The CoQ oxidoreductase FSP1 acts parallel to GPX4 to inhibit ferroptosis. Nature. 2019;575:688–92.
18. Mao C, et al. DHODH-mediated ferroptosis defence is a targetable vulnerability in cancer. Nature. 2021;593:586–90.
19. Kraft VAN, et al. GTP cyclohydrolase 1/tetrahydrobiopterin counteract ferroptosis through lipid remodeling. ACS Cent Sci. 2020;6:41–53.
20. Hanahan D, Weinberg RA. Hallmarks of cancer: the next generation. Cell. 2011;144:646–74.
21. Chen X, Kang R, Kroemer G, Tang D. Broadening horizons: the role of ferroptosis in cancer. Nat Rev Clin Oncol. 2021;18:280–96.
22. Friedmann Angeli JP, Krysko DV, Conrad M. Ferroptosis at the crossroads of cancer-acquired drug resistance and immune evasion. Nat Rev Cancer. 2019;19:405–14.
23. Liang C, Zhang X, Yang M, Dong X. Recent progress in ferroptosis inducers for Cancer therapy. Adv Mater. 2019;31:e1904197.
24. Wang H, et al. Emerging mechanisms and targeted therapy of ferroptosis in cancer. Mol Ther. 2021;29:2185–208.
25. Conrad M, Pratt DA. The chemical basis of ferroptosis. Nat Chem Biol. 2019;15:1137–47.
26. Doll S, et al. FSP1 is a glutathione-independent ferroptosis suppressor. Nature. 2019;575:693–8.
27. Nakamura T, et al. Phase separation of FSP1 promotes ferroptosis. Nature. 2023;619:371–7.
28. Li B, Yang K, Liang D, Jiang C, Ma Z. Discovery and development of selective aldehyde dehydrogenase 1A1 (ALDH1A1) inhibitors. Eur J Med Chem. 2021;209:112940.
29. Wang M, et al. ALDH1A1 promotes immune escape of tumor cells through ZBTB7B-glycolysis pathway. Cell Death Dis. 2024;15:568.
30. Gorodetska I, et al. ALDH1A1 drives prostate cancer metastases and radioresistance by interplay with AR- and RAR-dependent transcription. Theranostics. 2024;14:714–37.
31. Wang Q, et al. Tamoxifen enhances stemness and promotes metastasis of ERalpha36(+) breast cancer by upregulating ALDH1A1 in cancer cells. Cell Res. 2018;28:336–58.
32. Liu C, et al. ALDH1A1 activity in Tumor-Initiating cells remodels Myeloid-Derived suppressor cells to promote breast Cancer progression. Cancer Res. 2021;81:5919–34.
33. Bian Y, et al. Targeting ALDH1A1 to enhance the efficacy of KRAS-targeted therapy through ferroptosis. Redox Biol. 2024;77:103361.
34. Wang H, Zhan Y, Peng S, Fan S, Wang W. Targeting ALDH1A1 to induce necroptosis in nasopharyngeal carcinoma. J Cancer. 2022;13:3515–25.
35. Genovese I, et al. Binding of doxorubicin to Sorcin impairs cell death and increases drug resistance in cancer cells. Cell Death Dis. 2017;8:e2950.
36. Kim SI, Lee HJ, Kim SS, Kwon YS, Chun W. Sequestration of Sorcin by aberrant forms of Tau results in the defective calcium homeostasis. Korean J Physiol Pharmacol. 2016;20:387–97.
37. Tuo H, et al. Sorcin induces gastric cancer cell migration and invasion contributing to STAT3 activation. Oncotarget. 2017;8:104258–71.
38. Yamagishi N, et al. Increased expression of Sorcin is associated with multidrug resistance in leukemia cells via up-regulation of MDR1 expression through cAMP response element-binding protein. Biochem Biophys Res Commun. 2014;448:430–6.
39. Shabnam B, et al. Sorcin a potential molecular target for Cancer therapy. Transl Oncol. 2018;11:1379–89.
40. Wang Y, et al. Soluble resistance-related calcium-binding protein participates in multiple diseases via protein-protein interactions. Biochimie. 2021;189:76–86.
41. Colotti G, et al. Sorcin, a calcium binding protein involved in the multidrug resistance mechanisms in cancer cells. Molecules. 2014;19:13976–89.
42. Li Z, et al. Sorcin regulate pyroptosis by interacting with NLRP3 inflammasomes to facilitate the progression of hepatocellular carcinoma. Cell Death Dis. 2023;14:678.
43. Li C, et al. Nanotechnology-integrated ferroptosis inducers: a Sharp sword against tumor drug resistance. J Mater Chem B. 2022;10:7671–93.
44. Zhang C, Liu X, Jin S, Chen Y, Guo R. Ferroptosis in cancer therapy: a novel approach to reversing drug resistance. Mol Cancer. 2022;21:47.
45. Battista T et al. Roles of Sorcin in drug resistance in cancer: one protein, many mechanisms, for a novel potential anticancer drug target. Cancers (Basel) 12 (2020).
46. Zamparelli C, et al. Activation of the cardiac Na(+)-Ca(2+) exchanger by Sorcin via the interaction of the respective Ca(2+)-binding domains. J Mol Cell Cardiol. 2010;49:132–41.
47. Xu X, et al. Aldehyde dehydrogenases and cancer stem cells. Cancer Lett. 2015;369:50–7.
48. Tiwari N, et al. A prospective study of association of cancer stem cell marker aldehyde dehydrogenase 1 with clinicopathological profile in lung carcinoma patients. Indian J Pathol Microbiol. 2018;61:489–94.
49. Schafer A, et al. Aldehyde dehydrogenase 1A1–a new mediator of resistance to Temozolomide in glioblastoma. Neuro Oncol. 2012;14:1452–64.
50. Chen X, et al. A noncanonical function of EIF4E limits ALDH1B1 activity and increases susceptibility to ferroptosis. Nat Commun. 2022;13:6318.
51. Wu Y et al. ALDH1-Mediated autophagy sensitizes glioblastoma cells to ferroptosis. Cells 11 (2022).
52. Wei Y, et al. ALDH1: A potential therapeutic target for cancer stem cells in solid tumors. Front Oncol. 2022;12:1026278.
53. Tsuruta F, et al. SCFFbl12 increases p21Waf1/Cip1 expression level through atypical ubiquitin chain synthesis. Mol Cell Biol. 2016;36:2182–94.
54. Nishiyama M, Nita A, Yumimoto K, Nakayama KI. FBXL12-Mediated degradation of ALDH3 is essential for trophoblast differentiation during placental development. Stem Cells. 2015;33:3327–40.
55. Postow L, Funabiki H. An SCF complex containing Fbxl12 mediates DNA damage-induced Ku80 ubiquitylation. Cell Cycle. 2013;12:587–95.
56. Zhao B, et al. Notch and the pre-TCR coordinate thymocyte proliferation by induction of the SCF subunits Fbxl1 and Fbxl12. Nat Immunol. 2019;20:1381–92.
57. Robson EJ, He SJ, Eccles MR. A panorama of PAX genes in cancer and development. Nat Rev Cancer. 2006;6:52–62.

58. Nasri Nasrabadi P, Martin D, Gharib E, Robichaud GA. The Pleiotropy of PAX5 gene products and function. Int J Mol Sci 23 (2022).
59. Kurimoto K, et al. PAX5 gene as a novel methylation marker that predicts both clinical outcome and cisplatin sensitivity in esophageal squamous cell carcinoma. Epigenetics. 2017;12:865–74.
60. Rodrigues T, Reker D, Schneider P, Schneider G. Counting on natural products for drug design. Nat Chem. 2016;8:531–41.
61. Guzman ML, et al. The sesquiterpene lactone parthenolide induces apoptosis of human acute myelogenous leukemia stem and progenitor cells. Blood. 2005;105:4163–9.
62. Kannaiyan R, Shanmugam MK, Sethi G. Molecular targets of Celastrol derived from thunder of god vine: potential role in the treatment of inflammatory disorders and cancer. Cancer Lett. 2011;303:9–20.
63. Shen W, et al. Celastrol inhibits oligodendrocyte and neuron ferroptosis to promote spinal cord injury recovery. Phytomedicine. 2024;128:155380.
64. Pan M, et al. Celastrol alleviated acute kidney injury by Inhibition of ferroptosis through Nrf2/GPX4 pathway. Biomed Pharmacother. 2023;166:115333.
65. Luo P, et al. Celastrol induces ferroptosis in activated HSCs to ameliorate hepatic fibrosis via targeting Peroxiredoxins and HO-1. Acta Pharm Sin B. 2022;12:2300–14.
66. Zhang D, et al. Celastrol binds to its target protein via specific noncovalent interactions and reversible covalent bonds. Chem Commun (Camb). 2018;54:12871–4.
67. Klaic L, Trippier PC, Mishra RK, Morimoto RI, Silverman RB. Remarkable stereospecific conjugate additions to the Hsp90 inhibitor Celastrol. J Am Chem Soc. 2011;133:19634–7.
68. Liu J, et al. An integrated TCGA Pan-Cancer clinical data resource to drive High-Quality survival outcome analytics. Cell. 2018;173:400–e416411.

Publisher's note